LAWRENCE
LIVERMORE
NATIONAL
LABORATORY

LLNL-JRNL-408744

Shear Wave Velocity Structure of Southern African Crust: Evidence for Compositional Heterogeneity within Archaean and Proterozoic Terrains

E. M. Kgaswane, A. A. Nyblade, J. Julia, P. H. G. M. Dirks, R. J. Durrheim, M. E. Pasyanos

November 17, 2008

Journal of Geophysical Research

Disclaimer

Shear Wave Velocity Structure of Southern African Crust: Evidence for Compositional Heterogeneity within Archaean and Proterozoic Terrains

Eldridge M. Kgaswane[1,3], Andrew A. Nyblade[2], Jordi Julià[2] , Paul H. G. M. Dirks[3], Raymond J. Durrheim[3,5] , Michael E. Pasyanos[4]

1. Council for Geoscience, 280 Pretoria Road, Private Bag X112, Pretoria, 0001, South Africa
2. Department of Geosciences, Pennsylvania State University, University Park, Pennsylvania, USA
3. School of Geosciences, University of the Witwatersrand, Private Bag 3, Johannesburg, 2050, South Africa
4. Lawrence Livermore National Laboratory, 7000 East Avenue, Livermore, CA 94550, USA
5. Council for Scientific and Industrial Research, cnr Rustenburg and Carlow Roads, Johannesburg, South Africa

Submitted to Journal of Geophysical Research, November 14, 2008

Abstract

Crustal structure in southern Africa has been investigated by jointly inverting receiver functions and Rayleigh wave group velocities for 89 broadband seismic stations spanning much of the Precambrian shield of southern Africa. 1-D shear wave velocity profiles obtained from the inversion yield Moho depths that are similar to those reported in previous studies and show considerable variability in the shear wave velocity structure of the lower part of the crust between some terrains. For many of the Archaean and Proterozoic terrains in the shield, S velocities reach 4.0 km/s or higher over a substantial part of the lower crust. However, for most of the Kimberley terrain and adjacent parts of the Kheis Province and Witwatersrand terrain, as well as for the western part of the Tokwe terrain, mean shear wave velocities of $\leq$ 3.9 km/s characterize the lower part of the crust along with slightly (~5 km) thinner crust. These findings indicate that the lower crust across much of the shield has a predominantly mafic composition, except for the southwest portion of the Kaapvaal Craton and western portion of the Zimbabwe

Craton, where the lower crust is intermediate-to-felsic in composition. The parts of the Kaapvaal Craton underlain by intermediate-to-felsic lower crust coincide with regions where Ventersdorp rocks have been preserved, and thus we suggest that the intermediate-to-felsic composition of the lower crust and the shallower Moho may have resulted from crustal melting during the Ventersdorp tectonomagmatic event at c. 2.7 Ga and concomitant crustal thinning caused by rifting.

1. Introduction

In this paper, we investigate variations in the crustal structure of Archaean and Proterozoic terrains in southern Africa using new estimates of crustal shear wave velocities. Previous studies have suggested that there may be a significant amount of variability in crustal structure across southern Africa (e.g. de Wit and Tinker, 2004). For example, Niu and James (2002) found that the lower crust around the Kimberley region in the western part of the Kaapvaal Craton has an intermediate-to-felsic composition, and from this finding, they suggested that the lower crust beneath much of the Kaapvaal Craton could be dominated by intermediate-to-felsic lithologies. Studies by Nguuri (2004) and Nair et al. (2006), however, show crustal Vp/Vs ratios as high as 1.78 for parts of the Kaapvaal Craton and surrounding Proterozoic mobile belts, suggesting that in some areas the crust may contain a significant proportion of mafic rock. The presence of mafic lithologies within Precambrian crust has also been found in other regions of Africa, such as the Archaean Tanzania Craton and Neoproterozoic Mozambique Belt in East Africa (Julià et al., 2005).

Characterizing the variability in crustal structure across southern Africa is important for improving our understanding of Precambrian crustal growth and tectonics. Many studies show that the composition of the lower crust remains the largest uncertainty in determining the overall

composition and structure of the crust, and this can lead to uncertainty in the role of the lower crust in continental tectonics (Christensen and Mooney, 1995; Rudnick and Fountain, 1995, Rudnick and Gao, 2003).

To investigate details of crustal structure in southern Africa, we have jointly inverted receiver functions and Rayleigh wave group velocities for 101 broadband seismic stations spanning the greater part of the exposed Precambrian shield of southern Africa (Figures 1 and 2). A total of 71 teleseismic earthquakes were used to compute the receiver functions and Rayleigh wave group velocities in the period range of 10 – 175 sec were taken from both regional surface wave tomographic results and global models. From the joint inversion, 1-D shear wave velocity profiles for the crust and uppermost mantle beneath 89 stations have been obtained. The shear wave velocity profiles indicate that the lower crust across much of the Kaapvaal and southern Zimbabwe Cratons and of the surrounding mobile belts has a predominantly mafic composition, with the exception of the southwest portion of the Kaapvaal Craton (central part of the Kimberley terrain) and western portion of the Zimbabwe Craton (western part of the Tokwe terrain) where the lower crust is intermediate-to-felsic in composition. The intermediate-to-felsic composition within the Kimberley terrain is consistent with results reported by Niu and James (2002). The implication of this finding for the tectonic history of the Kimberley terrain and neighbouring terrains is examined vis-à-vis the major Precambrian tectonothermal events to have affected southern Africa.

2. Tectonic and geological framework of southern Africa

2.1 Overview of Precambrian structure

The Kalahari Craton, which forms the nucleus of the southern African shield, is comprised of the Archaean Kaapvaal Craton welded to the Archaean Zimbabwe Craton by the

Archaean and Palaeoproterozoic Limpopo Belt (de Wit et al., 1992) (Figure 1). The Kalahari Craton is bounded by the Palaeoproterozoic Okwa-Magondi Belt to the northwest, the Mesoproterozoic Namaqua-Natal Belt including Kheis Province to the south and southwest, and the Palaeozoic Cape Fold Belt to the south (Figure 1). A brief description of these tectonic terrains follows.

2.2 Kaapvaal Craton

The Kaapvaal Craton is an Archaean granite-greenstone terrain that formed between 3.7 and 2.7 Ga (de Wit et al., 1992; Eglington and Armstrong, 2004). Based on the age distribution of supracrustal and intrusive rocks the craton has been subdivided into four tectonostratigraphic terrains; the Kimberley (3.0 – 2.8 Ga), the Pietersburg (3.0 – 2.8 Ga), the Witwatersrand and Swaziland terrains (3.6 – 3.1 Ga) separated by the Thabazimbi-Murchison and Colesburg lineaments and the Inyoka Fault (Figure 1) (Eglington and Armstrong, 2004). The Swaziland terrain is the oldest (> 3.2 Ga) and the Witwatersrand terrain was accreted to it at ~3.2 Ga. The Pietersburg and Kimberely terrains were joined to the Witwatersrand-Swaziland terrain between 3.0 and 2.8 Ga. A series of rift-related, intracratonic basins, including the Dominion (3.1 Ga), Witwatersrand (3.0 – 2.8 Ga), Ventersdorp (2.7 Ga), Transvaal (2.6 – 2.2 Ga) and Waterberg (2.0 – 1.8 Ga) basins, developed within the Kaapvaal Craton, which experienced a last major tectonothermal disturbance with the emplacement of the Bushveld Complex (2.05 Ga) (Eglington and Armstrong, 2004; Johnson et al., 2006).

2.3 Zimbabwe Craton

The Zimbabwe Craton consists of granite-greenstone terrains that formed between 3.6 – 2.5 Ga (e.g. Dirks and Jelsma, 2002). The Zimbabwe Craton is characterized by three stages of crustal formation. The Tokwe Gneiss terrain in the centre of the craton, formed at 3.6 – 3.3 Ga, contains mafic fragments that represent the remnants of highly deformed and metamorphosed

99 greenstone belts. A sequence of clastic sediments and greenstones accreted against the old
100 Tokwe Gneiss terrain between 3.2 – 2.8 Ga. The principal period of greenstone formation and
101 accretion occurred between 2.7 – 2.6 Ga, with stabilization of the craton around 2.6 Ga. The
102 Great Dyke was emplaced around 2.58 Ga, marking the last major tectonothermal event to affect
103 the craton (Jelsma and Dirks, 2002).

104 **2.4 Limpopo Belt**

105 The Limpopo Belt is a roughly east-west trending zone of high-grade metamorphic rocks
106 that separates the Kaapvaal and Zimbabwe Cratons (e.g. McCourt and Armstrong, 1998;
107 Kramers et al., 2006). The belt has been subdivided into three domains, the Northern Marginal
108 Zone (NMZ), the Central Zone (CZ) and the Southern Marginal Zone (SMZ), separated by major
109 shear zones (Kramers et al., 2006). The NMZ and SMZ contain remnants of Archaean granite-
110 greenstone terrains that were modified by a major orogenic event at 2.6 – 2.5 Ga during which
111 the rocks attained amphibolite to granulite facies metamorphism (e.g. Berger et al., 1995;
112 Kreissig et al., 2000; Kramers et al., 2006). The CZ (> 3.0 & 2.6 & 2.0 Ga) is dominated by
113 granulite facies gneiss with minor metasedimentary and ultramafic intercalations (e.g. Barton et
114 al., 1979; Kramers et al., 2006) affected by orogenic activity at 2.6 – 2.5 Ga and then again,
115 importantly, at 2.0 Ga, during which the CZ, the NMZ and the SMZ attained their current
116 configuration.

117 **2.5 Bushveld Complex**

118 The Bushveld Complex (2.05 Ga) is the world's largest known layered mafic intrusion,
119 extending >350 km in both north-south and east-west directions and reaching a vertical thickness
120 of about 8 km (e.g., Webb et al., 2004). The Bushveld Complex (BC) intruded into the northern
121 part of the Kaapvaal Craton (Figure 1) and has been subdivided into the Rustenburg Mafic
122 Layered Suite, the Lebowa Granite Suite, the Rashoop Granophyre Suite, and the Rooiberg

123 Group, which consists of rhyolites and basaltic andesites (SACS, 1980; Hatton and Schweitzer,
124 1995; Cawthorn et al., 2006).

125 **2.6 Mesoproterozoic to Palaeozoic mobile belts**

126 The Magondi Belt is dominated by a passive margin, shelf sediments of the Magondi
127 supergroup exposed to the northwest of the Zimbabwe Craton (McCourt et al., 2001) and
128 thrusted eastward onto the craton during the Magondi Orogeny (~2.0 – 1.8 Ga). Magondi Belt
129 rocks have been correlated with deformed mafic and felsic magmatic rocks of the 2.05 Ga Okwa
130 terrain in the central north Botswana (Figure 1) (Stowe, 1989), suggesting the presence of a
131 continuous north-trending orogenic belt to the west of the Zimbabwe Craton, possibly merging
132 with the CZ of the Limpopo Belt.

133 The Namaqua-Natal Belt (NNB) comprises igneous and supracrustal rocks to the south
134 and west of the Kaapvaal Craton, that accreted against the craton during the Namaqua Orogeny
135 (1.2 – 1.0 Ga). The central part of the belt is covered by younger sediments of the Karoo
136 Supergroup, leaving outcrop to the west (the Namaqua Sector) and south-east (the Natal Sector)
137 of the craton (Cornell et al., 2006). The Namaqua Sector is composed of five distinct, 2.0 to 1.3
138 Ga terrains, separated from the Kaapvaal Craton by a passive margin sequence of siliciclastic
139 rocks of the Olifantshoek Supergroup (2.0 – 1.7 Ga), referred to as the Kheis Province (Cornell
140 et al., 2006). Accretion of the Namaqua Sector at 1.0 – 1.2 Ga coincided with eastward thrusting
141 of Olifantshoek sediments onto the craton (Moen, 1999; Eglington and Armstrong, 2004)
142 resulting in a thin-skinned fold-and-thrust belt also called the Kheis Belt and erroneously
143 correlated with the 2.0 Ga Okwa terrain and Magondi Belt to the north (e.g. Stowe, 1986).

144 The Cape Fold Belt (CFB) comprises a siliciclastic passive margin sequence of the Cape
145 Supergroup (500 – 330 Ma) (Thamm and Johnson, 2006) deformed in a northeast verging fold-
146 and-thrust belt during the Cape Orogeny (~ 278 – 245 Ma). The belt is thought to have formed as

147 a result of a subduction zone along the southern margin of the Gondwana supercontinent (e.g.
148 Ransome and de Wit, 1992; Newton et al., 2006).
149

150 ## 3. Seismic structure of southern African crust

151 Early studies of the crust in the Kaapvaal Craton mainly used seismic recordings of mine
152 tremors associated with gold mining activity in the Witwatersrand basin (e.g., Gane et al., 1949;
153 Willmore et al., 1952; Gane et al., 1956; Hales and Sacks, 1959). Hales and Sacks (1959) shows
154 a two-layered crust in the eastern Kaapvaal Craton with a Moho depth of 37 km, and an upper
155 crustal layer ~ 24 km thick with P and S velocities of 6.0 and 3.6 km/s, respectively. They also
156 found a lower crustal layer ~ 13 km thick with P and S velocities of 7.0 and 4.0 km/s,
157 respectively. An early surface wave study carried out by inverting for Rayleigh and Love wave
158 group and phase velocities from regional earthquakes obtained a Poisson's ratio of 0.28 for the
159 lower crust in the northern Kaapvaal Craton and a crustal thickness in the range of 40 – 45 km
160 (Bloch et al., 1969). The first seismic refraction studies in and around the Witwatersrand basin
161 yielded a crustal thickness of 35 km and lower crustal P-wave velocities in the range of 6.4 to 6.7
162 km/s (Durrheim and Green, 1992). A similar study by Green and Durrheim (1990) of the NNB
163 indicated a Moho depth of 42 km and P-wave velocities in the range 6.6 to 6.9 km/s for the
164 lower crust.

165 More recently, our understanding of crustal structure in southern Africa has been
166 advanced by studies using data from the Southern African Seismic Experiment (SASE) (Carlson
167 et al., 1996). A compilation of results from Harvey et al. (2001), Nguuri et al. (2001),
168 Stankiewicz et al. (2002), Niu and James (2002), James et al. (2003), Kwadiba et al. (2003),
169 Wright et al. (2003), Webb et al. (2004), and Nair et al. (2006) show crustal thicknesses of 35 –
170 45 km and 34 – 37 km, respectively, for the Kaapvaal and Zimbabwe cratons. The studies

171 reported Moho depths for the Kheis Province, BC, Limpopo Belt, Okwa/Magondi Belt, NNB
172 and CFB of 40 km, 40 – 53 km, 37 – 55 km, 40 – 45 km, 40 – 50 km and 26 – 45 km,
173 respectively.

174 Nguuri (2004) and Nair et al. (2006) reported variable Vp/Vs ratios for a number of
175 crustal terrains across southern Africa (Table 1) and interpreted Vp/Vs ratios > 1.76 to be
176 indicative of mafic and ultramafic lithologies in the crust. The differences in the Vp/Vs ratio for
177 some terrains, as well as the number of stations used to compute the average ratios, reflect
178 different selections of geographic regions and data in the two studies. One of the most detailed
179 investigations of crustal structure in the Kaapvaal Craton has been undertaken by Niu and James
180 (2002) for a small area in the Kimberley terrain using data from the Kimberley seismic array.
181 Niu and James (2002) obtained for the lowermost crust P and S velocities of 6.75 and 3.90 km/s,
182 respectively, and a Poisson's ratio of 0.25, indicating an intermediate-to-felsic for the lowermost
183 crust. These findings suggest a lowermost crust with an intermediate-to-felsic composition.
184 They also found sharp (i.e., less than 0.5 km wide) and flat (i.e., topographic relief less than 1
185 km) Moho. Petrologic studies of the Kimberley area by Schmitz and Bowring (2003a,b) show
186 that mafic granulites are absent from lower-crustal xenolith suites, consistent with the findings
187 by Niu and James (2002).
188

189 ## 4. Sources of data

190 Data from a total of 101 broadband stations have been used in this study to compute
191 receiver functions. The 101 stations belong to the SASE network, the AfricaArray (AA)
192 network, the South African National Seismograph Network (SANSN) and the Global Seismic
193 Network (GSN) (Figure 2). The SASE network consisted of 82 stations over 2 years (1997 –
194 1999) spanning much of the Kalahari Craton along a NE-SW axis (Figure 2). Data from five

195 stations in the Kimberley array (1999), which was deployed as a high resolution extension to the
196 SASE network (Niu and James, 2002), have also been used. The AA network began operation in
197 2006 and consists of 29 permanent seismic stations spread across eastern and southern Africa.
198 More than 1 year of data from eleven of the AA stations in southern Africa were used for this
199 study (Figure 2).

200 A total of 71 teleseismic earthquakes with epicentral distances of 30° and 99° recorded by
201 the above-mentioned 101 stations were selected from an original list of 84 earthquakes for
202 computing receiver functions (Figure 3). The selected earthquakes have surface-wave
203 magnitudes ranging from 6.0 to 8.2. A table with the event details is provided as supplemental
204 material.

205 Rayleigh wave group velocities used in this study have been taken from Pasyanos and
206 Nyblade (2007) for periods of 10 to 90 sec, and from the Harvard model for a period range of 90
207 to 175 sec (Larson and Ekström, 2001). A single dispersion curve for each station was obtained
208 by joining the group velocities from 10 to 90 sec and 90 to 175 sec and smoothing the composite
209 curve using a 3-point running average.

210

211 ## 5. Data processing and modelling methodology

212 ### 5.1 Receiver functions

213 Receiver functions were computed using the iterative deconvolution method of Ligorría
214 and Ammon (1999), after deconvolving the vertical components of teleseismic P-wave
215 recordings from the corresponding radial and transverse components. The deconvolution
216 procedure equalizes the teleseismic waveforms so that near-source and instrumental effects are
217 removed from the resulting time series (Langston, 1979). Only the radial receiver functions were
218 used in the joint inversion with the Rayleigh wave group velocity curves; the transverse receiver

functions are identically zero for isotropic and laterally homogeneous media, and were computed to verify that this holds for the medium under each station.

For each station, receiver functions were binned within ray parameter groups from 0.04 to 0.049 s/km, 0.05 to 0.059 s/km and 0.06 to 0.069 s/km. The purpose of grouping the receiver functions according to ray parameter is to properly account for the phase moveout due to varying incidence angles (Cassidy, 1992; Gurrola and Minster, 1998). Receiver function averages were then computed for each ray parameter bin.

For each teleseismic event, receiver functions were computed at two overlapping frequency bands: a low frequency band of $f \leq 0.5$ Hz (Gaussian bandwidth of 1.0 s), and a high frequency band of $f \leq 1.25$ Hz (Gaussian bandwidth of 2.5 s). The low frequency bandwidth provides a better constraint on longer wavelength features in the subsurface, while the high frequency bandwidth provides a better constraint on shorter wavelength features. The combination of low and high frequency receiver functions help in discriminating sharp versus gradational transitions in the subsurface (Owens and Zandt, 1985; Julià, 2007).

5.2 Joint inversion of receiver functions and Rayleigh wave group velocities

The joint inversion of receiver functions and surface wave dispersion curves results in 1-D shear wave depth-velocity profiles for each recording station (Julià et al., 2000, 2003). The technique has been widely used to investigate crustal and upper mantle structure in other continental regions, for example, the Arabian shield (Julià et al., 2003), the Tanzania Craton (Julià et al., 2005) and the Ethiopian Plateau (Dugda et al., 2006). The advantage of jointly inverting receiver functions and surface wave dispersion measurements is that a better resolution of the subsurface shear wave velocity structure can be obtained compared to when either data set is inverted independently (Julià et al., 2000, 2003).

A critical condition implicit in the joint inversion is that the two data sets must sample the same region. At crustal and uppermost mantle depths, receiver functions sample structures laterally within a radius similar to the crustal thickness. Given this, the receiver function averages at each station were jointly inverted with the dispersion velocities corresponding to the 1 degree x 1 degree grid cell in the surface wave tomography that enclosed the station.

The joint inversion method makes use of a linearized inversion procedure that minimizes a weighted combination of the L2 norm of the vector residuals corresponding to each data set. The weights consist of a normalization constant that accounts for the different number of data points and different physical units in each data set, as well as an influence parameter that controls the relative influence of each data set on the inverted model (Julià et al., 2000). In order to obtain smoothly varying depth-velocity profiles, the objective function also includes a model vector-difference norm of the second order differences between adjacent layers (Ammon et al., 1990; Julià et al., 2000).

Influence factors and smoothing parameters were selected for each tectonic domain in order to obtain smooth depth-velocity profiles that match the observations. For most of the stations, a good fit to the data was obtained for an influence factor of 0.5 and a smoothing parameter from zero to 0.2. The smoothing parameter had to be raised as high as 0.3 for some of the stations within the mobile belts, suggesting a greater degree of small-scale heterogeneity.

The model parameterization consisted of 74 layers extending to a depth of 532 km. Layer thicknesses of 1 and 2 km were used for the first and second layer, 2.5 km between 3 and 60.5 km depth, 5 km between 60.5 and 255.5 km depth, and 17 to 40 km below 255.5 km depth. The increase in layer thicknesses with depths corresponds to a decrease in the resolving power of the dispersion velocities with increasing period. The starting model used for the inversions is the PREM model (Dziewonski and Anderson, 1981) modified for continental structure above 60.5

km depth (see Figure 4). Poisson's ratio in the starting model was set at 0.25 in the crust and mantle to a depth of 86 km, 0.28 between depths of 86 – 230 km, 0.29 between depths of 230 – 374 km, 0.30 between depths of 374 – 430 km and 0.29 between depths of 430 – 532 km. Densities were obtained from P-wave velocities using the empirical relationship of Berteussen (1977).

5.3 Starting model dependence and trade-offs

To test the dependence of the inversion results on the starting model, a range of regional models were used as starting models for the inversion (Qiu et al., 1996; Zhao et al., 1999; Simon et al., 2002; Li and Burke, 2006). P-wave velocities were computed using the same Vp/Vs ratio as for the starting model. The outcome of this test, illustrated in Figure 4, shows that the inversion results in the 0 – 60 km depth range are not sensitive to the starting models. We observed, however, that there is a trade-off between velocities at depths of ~ 60 – 150 km with those below 200 km. To constrain this trade-off, we forward modelled structure below 200 km depth using a trial-and-error process by finding models that best fit the 140 – 175 sec period group velocities. This was done by fixing velocities below 200 km between a range of -5 and +5% of the PREM velocities (Dziewonski and Anderson, 1981) and then inverting for the velocity structure above 200 km depth.

The best fitting model for each station was selected when the predicted group velocities in the 140 – 175 sec range matched the observed group velocities. Figure 5 shows an example for one station with velocities of PREM and -2, -3, -5% PREM below 200 km depth. The best fitting model for this station is -3% PREM. For most of the stations, it was found that a -2% PREM model tends to fit the 140 – 175 sec period group velocities best. However, a -3% PREM model was used for the stations in the Kheis Province, Limpopo Belt, Okwa terrain and Zimbabwe Craton and a -5% PREM model was used for both the NNB and CFB.

290 **5.4 Model uncertainties**

291 Following the approach by Julià et al. (2005), the uncertainties in the joint inversion
292 results were estimated by repeating inversions for each station using a range of weighting
293 parameters, constraints and Poisson's ratio. The uncertainties in the shear wave velocities for the
294 crust and uppermost mantle are around 0.1 km/s. As discussed in the next section, the most
295 relevant findings of this study concerns lower crustal structure. Therefore, to assess further the
296 accuracy to which lower crustal velocities are constrained in our joint inversion models, we
297 evaluated the uncertainty in our models by running velocity-constrained inversions over depth
298 ranges of interest. To illustrate this approach, we have selected two stations representing our
299 end-member models in lower crustal structure: station BOSA, in the Kimberley terrain, with
300 slow lower crustal velocities of ~ 3.8 km/s; and station SUR, in the NNB, with fast lower crustal
301 velocities around 4.3 km/s. We then ran our constrained joint inversions using exactly the same
302 parameters and starting models as in the original inversions, but with the additional requirement
303 that velocities be faster, (~ 4.0 km/s), between 15 – 33 km depth for BOSA, and slower, (~ 3.8
304 km/s), between 20 – 40 km depth for SUR.

305 The results of the joint inversion for the two stations are shown in Figure 6. For station
306 SUR neither the predicted Ps nor the PpPms phase fit the observed phases, both falling outside
307 the 1-sigma error bounds of the receiver functions, while for station BOSA the predicted Ps
308 phase does not fit the observed Ps phase. In addition, the predicted Rayleigh wave group
309 velocities tend to lie either below or above the error bounds of the observed group velocities for
310 both stations in the 10 – 60 sec period range, which includes the periods most sensitive to the
311 lower crustal structure. Hence, lower crustal velocities of < 4.0 km/s for BOSA and ≥ 4.0 km/s
312 for SUR are required to match dispersion velocities in the 10 – 60 sec period range, a result that
313 is consistent with our uncertainty estimates of $\pm$ 0.1 km/s for depths above 60 km in our models.

Changing Poisson's ratio in the crust of the starting model did not change the joint inversion results.

6. Results

For twelve of the stations, the inversions did not yield good fits to the receiver functions and therefore results for these stations are not presented or interpreted. The receiver functions are too noisy to obtain good waveform fits at stations SA01, SA02, SA03, SA58, SA69, SA82, SA139, SA155, CNG, while it is difficult to see a Moho Ps conversion on the receiver functions for stations SA07, SA08, SA12 (all in the NNB). The results for the remaining 89 stations are summarized in Figures 7 -12. More detailed results, including waveform fits, are provided as supplemental material.

Firstly, we focus on crustal thickness, which we determined for each station by placing the Moho at the depth where Vs increases to 4.4 – 4.5 km/s. Given the ± 0.1 km/s uncertainty in Vs for each layer in our models above 60 km depth, and the smoothly varying nature of the Vs profile for some stations, the uncertainty in defining Moho depth is 2.5 km for most stations and up to 5 km for stations with a gradational Moho. Within the reported uncertainties, we find a 1-to-1 correlation between our Moho estimates and those reported by Nguuri et al. (2001), Nguuri (2004) and Nair et al. (2006), except for a handful of stations shown in Figure 7 with solid symbols. Two stations (SA49 and SUR) lie more than 5 km above the 1-to-1 correlation line, where our estimates of Moho depth are about 5 to 10 km less than those reported by Nair et al. (2006). The differences can be explained by the fact that the velocity profiles for both stations exhibit a gradational Moho. Nine stations lie more than 5 km below the 1-to-1 correlation line, where our estimates of Moho depth are about 5 km greater than those reported by Nguuri et al. (2001), Nguuri (2004) and Nair et al. (2006). The velocity profiles for these stations (SA34,

SA28, SA46, SA48, SA47, SA16, SA70, SA10) show complicated lowermost crustal structure commonly with a gradational Moho.

Next we examine variations in the shear wave velocity structure of the crust. Shown in Figures 8a – d are the velocity profiles grouped by tectonic terrain within the Kaapvaal and Zimbabwe Cratons and surrounding orogenic belts. Table 2 provides a summary of key crustal parameters. From visual inspection of the 89 shear wave velocity profiles and from the summary of crustal parameters in Table 2, we observe distinct crustal characteristics in many terrains.

6.1 Variability in lower crustal structure

The primary difference between terrains is in the velocity structure of the lower part of the crust. For most terrains, S velocities reach 4.0 km/s or higher over a substantial part of the lower crust. This is illustrated in columns 7 and 8 of Table 2, which show mean velocities below 20 and 30 km depth for each terrain. The central part of the Kimberley terrain and the western part of the Tokwe terrain, however, are different. Here mean velocities of $\leq$ 3.9 km/s occur in the lower part of the crust (columns 7 and 8, Table 2). This variability in lower crustal structure is also illustrated in column 9 of Table 2, which shows the average thickness of crustal layers with Vs $\geq$ 4.0 km/s. All terrains except for the central part of the Kimberley terrain and the western part of the Tokwe terrain have, on average, greater than 5 km of high velocity (Vs $\geq$ 4.0 km/s) rock within the lower part of the crust.

The variability in lower crustal structure is illustrated further in Figures 9 and 10. In Figure 9, the spatial variability in lower crustal velocity structure is shown in two ways for 1 x 1 degree blocks. First, the mean shear wave velocity below 30 km depth is indicated with shaded boxes, and superimposed on the boxes are symbols showing the thickness of lower crustal layers with Vs $\geq$ 4.0 km/s. The anomalous nature of lower crustal structure in the central part of the Kimberley terrain and the western part of the Tokwe terrain is readily apparent. It can also be

362 seen that the anomalous region of lower crustal structure extends beyond the central region of the
363 Kimberley terrain into the western part of the Witwatersrand terrain and the eastern part of the
364 Kheis Province. The lack of high velocity rock in the lower parts of the crust in these terrains
365 can also be seen by visual inspection of Figure 8, where a reference line of 4.0 km/s has been
366 drawn on each velocity profile to highlight the variability in lower crustal velocities. The gray
367 shading shows layers in the lower crust with Vs $\geq$ 4.0 km/s.

368 A related observation is that the regions with lesser amounts of high velocity rock in the
369 lower parts of the crust tend to have a shallower Moho. Figure 10 shows crustal thickness plotted
370 against the average shear wave velocity below 30 km depth for 88 stations (station SA04, where
371 we find 28 km thick crust, is left off the graph). The plot shows two linear fits, one for stations
372 with crustal thicknesses less than 40 km and one for stations with crustal thicknesses greater
373 than 40 km. While there is some scatter in the plot, a clear trend can be seen where the stations
374 with the thinner crust (~34 – 40 km) have average shear wave velocities mostly less than 4.0
375 km/s. Stations underlain by thicker crust (> 40 km) have average shear wave velocities about or
376 greater than 4.0 km/s. Most of the areas with a deeper Moho and thicker layers of high velocity
377 rock in the lower part of the crust are located in four terrains, the CZ of the Limpopo Belt, the
378 NNB, the BC, and the Kheis Province.

379 In Figure 11 we display the receiver functions and dispersion curves for two
380 representative stations to illustrate that there are appreciable differences in the data that give rise
381 to the variability in the lower crustal structure in our models. The model for station SA81 in the
382 NNB shows a mean Vs $\geq$ 4.1 km/s below 20 km depth and a Moho at 46 km depth. The model
383 for station BOSA in the central part of Kimberley terrain shows a mean Vs < 4.0 km/s below 20
384 km depth and a Moho at 36 km depth. The receiver functions for station BOSA shows a Moho
385 Ps conversion and multiple (PpPms) with larger amplitudes than the receiver functions for

station SA81. The dispersion curve for station BOSA also shows lower group velocities than the curve for station SA81 for periods sensitive to lower crustal structure (~15 – 40 sec).

6.2 Variability in upper crustal structure

A high velocity zone in the upper crust at depths < 15 km can be seen in the velocity models for a number of stations (Figure 8). The high velocity zones are isolated features seen on one or two stations in some of the terrains (e.g., station SA61 in the Okwa terrain), but for the NNB, a high velocity zone in the upper crust is found beneath all stations (Figure 8c). Shear velocities within these zones are consistently in the range of 3.7 - 4.0 km/s or less than 3.7 km/s (e.g. station SA76 in the eastern Tokwe terrain, Figure 8a).

6.3 Mantle velocities

For most of the terrains within both the cratonic areas and mobile belts, the mean S velocity from the Moho to depths of ~60 km is between 4.5 and 4.7 km/s (column 5, Table 2). The NNB shows slightly higher velocities of 4.8 km/s. We find little evidence for systematic differences in the uppermost mantle velocities across southern Africa. Deeper mantle structure is not sufficiently resolved to comment on variations in lithospheric thickness or sublithospheric mantle structure.

7. Discussion

In this section, we interpret the variability in crustal structure described in section 6 and discuss possible explanations for its origin. Because southern Africa has not experienced a major tectonothermal event since the Karoo flood basalt volcanism at c. 180 Ma, the velocity variability found within the crust most likely results from compositional differences rather than thermal ones. It is well established from laboratory studies that mafic lithologies commonly found in the continental crust have higher shear wave velocities (> 3.9 km/s) while intermediate-

410 to-felsic lithologies have lower shear wave velocities (< 3.9 km/s) (e.g., Holbrook et al., 1992;
411 Christensen and Mooney, 1995; Rudnick and Fountain, 1995; Rudnick and Gao, 2003).
412 Common mafic lower crustal lithologies include amphibolite, garnet-bearing and garnet-free
413 mafic granulite, and mafic gneiss (e.g., Rudnick and Fountain, 1995; Rudnick and Gao, 2003).

414 **7.1 Interpretation of high Vs in the lower crust**

415 We interpret the crustal layers in our models with shear wave velocities of 4.0 km/s or
416 higher as consisting of predominantly mafic lithologies. Rudnick and Fountain (1995) and
417 Rudnick and Gao (2003) argued that high velocity rock (Vp ~ 7.0 km/s, Vs ~ 4.0 km/s) is
418 characteristic of the lower crust in many Precambrian terrains globally. Thus, our interpretation
419 is not unprecedented.

420 Rudnick and Gao (2003) also suggest several explanations for the origin of mafic lower
421 crust in Precambrian terrains, such as basaltic underplating, magmatic intrusion, and
422 tectonomagmatic processes responsible for the formation of Archaean crust. The mafic layer in
423 the lower crust of the BC, which exceeds 15 km in thickness, is likely caused by a combination
424 of magmatic intrusion and underplating. It has been estimated that the total magma volume that
425 has been added to the Bushveld crust is around 0.6×10^6 km^3 (Von Gruenewaldt et al., 1985),
426 adding ~5-10 km to the thickness of the crust. The large (> 10 km) thickness of mafic rock in
427 the lower parts of the crust in the NNB, the CZ of the Limpopo Belt, parts of the Kheis Province
428 and the CFB can be attributed to suture processes during the formation of these terrains. In
429 Precambrian sutures elsewhere (e.g., the Superior Province - Gibb et al., 1983; the Tanzania
430 Craton - Nyblade and Pollack, 1992; the Yilgarn Craton - Mathur, 1974, Wellmann, 1978; the
431 Indian shield - Subrahmanyam, 1978; the Mann shield - Blot et al., 1962, Louis, 1978, Black et
432 al., 1979), 5 -10 km of crustal thickening is observed along with the presence of mafic units in a
433 crust commonly affected by granulite facies metamorphism and extraction of a felsic partial melt

component. Both the thicker crust and the large thickness of high Vs lower crust found in the NNB, CZ, and Kheis Province is consistent with typical "suture" thickened crust found in other Precambrian terrains, and need not be viewed as anomalous.

The Vp/Vs ratios from Nguuri (2004) and Nair et al. (2006) (Table 1) are in reasonable agreement with our interpretation. The mafic lower crust we find in the BC is consistent with the Vp/Vs ratios for both studies that are > 1.76. For the NNB and Limpopo Belt, the mafic lower crust that we find is consistent with the reported Vp/Vs ratios of 1.78 and 1.84, respectively.

7.2 Interpretation of low Vs in the lower crust

Following the experimental studies of rock velocties discussed above, we interpret the lower shear wave velocities ($Vs \leq 3.9$ km/s) in the lower parts of the crust in several terrains to indicate the presence of predominantly intermediate-to-felsic lithologies. The lack of mafic material in the lower crust and the mean crustal thickness of 36 km for the central block of the Kimberley terrain are consistent with the findings by Niu and James (2002), which are, however, limited to a 2400 km^2 region around Kimberley town. Our results indicate that the region of low Vs in the lower crust extends across much of the Kimberley terrain and into parts of the adjacent Kheis Province and Witwatersrand terrain (Figure 9).

To explain an intermediate-to-felsic composition for the lower crust in the Kimberley terrain, as well as the flat Moho that Niu and James (2002) observed, James et al. (2003) suggested that the crust could have been extensively remelted during the Ventersdorp tectonomagmatic event c. 2.7 Ga. This possibility is supported by Schmitz and Bowring (2003a,b), who observed 2.7 Ga, ultra-high temperature metamorphic assemblages in lower crustal xenoliths from kimberlite pipes intruded into the western part of the Kaapvaal Craton.

Melting of the lower crust during the Ventersdorp event may not have resulted in the removal of the lower mafic crust unless accompanied by concomitant thinning. Figure 12 shows the distribution of the Ventersdorp Supergroup superimposed on lower crustal velocity variations. Most of the areas underlain by intermediate-to-felsic lower crust coincide with the region where Ventersdorp rocks have been preserved. Using seismic reflection profiles, de Wit and Tinker (2004) describe Ventersdorp age half graben systems within the upper crust across the central Kimberley and Witwatersrand terrains. The half-grabens are characterized by asymmetrical listric faults that trend between east and southeast and de Wit and Tinker (2004) argued that the listric faults are associated with thinning of underlying lower crust. Consequently, regions in the Kaapvaal Craton underlain by an intermediate-to-felsic lower crust may reflect areas where mafic lower crust was either thinned or removed during the Ventersdorp event. A similar explanation could be invoked for the low Vs observed in the lower crust in the western part of the Tokwe terrain, which is overlain by a 3.1 – 2.95 Ga transgressive passive margin and rift sequences (Jelsma and Dirks, 2002).

7.3 Crustal xenoliths

Lower crustal xenoliths in southern Africa are most commonly found within kimberlite pipes (e.g. Dawson, 1980, Nixon, 1987; Schmitz and Bowring, 2003) (Figure 12). Cratonic lower crustal granulite xenoliths have been described from the Kimberley region (1), NNB (2, 3, 4, 5, 6), Free State province (7, 8, 9, 10), northern Lesotho (11, 12, 13) (Schmitz and Bowring, 2003). Off-craton and craton-margin xenoliths come from the CZ of the Limpopo Belt (14) (Pretorius and Barton, 2003) and the unexposed extension of the Magondi Belt in the north-central Botswana (15) (Schmitz and Bowring, 2003a).

Mafic granulites are absent in lower-crustal xenolith suites from the Kimberley terrain, which are dominated by metapelite and some preserving ultra-high temperature granulite

481 assemblages. However, mafic granulite xenoliths are common at all of the other localities
482 (Dawson and Smith, 1987; Dawson et al., 1997; Schmitz and Bowring, 2003a,b). The absence of
483 mafic xenoliths in the Kimberley terrain and the presence of mafic xenoliths in the other terrains
484 is consistent with the variability in the shear velocity structure of the lower crust found in this
485 study.
486

487 ## 8. Summary

488 To investigate details of crustal structure in southern Africa, we have jointly inverted
489 receiver functions and Rayleigh wave group velocities for 89 broadband seismic stations
490 spanning the greater part of the exposed Precambrian shield of southern Africa. From the joint
491 inversion, 1-D shear wave velocity profiles for the crust and uppermost mantle beneath the
492 stations have been obtained.
493 Within the reported uncertainties, we find a 1-to-1 correlation between our Moho depth
494 estimates and those reported by previous studies. The primary new observation that we make is
495 that there is a considerable difference between some terrains in the velocity structure of the lower
496 part of the crust. For most Archaean and Proterozoic terrains, S velocities reach 4.0 km/s or
497 higher over a substantial part of the lower crust. However, for much of the Kimberley terrain and
498 adjacent parts of the Kheis Province and Witwatersrand terrain, as well as for the western part of
499 the Tokwe terrain, mean shear wave velocities of $\leq$ 3.9 km/s characterize the lower part of the
500 crust along with slightly (~5 km) thinner crust. The lower shear velocities in the lower crust of
501 the Kimberley terrain and the shallower Moho are consistent with results from previous studies.
502 We find little evidence for systematic differences in the uppermost mantle velocities across
503 southern Africa. Deeper mantle structure is not sufficiently resolved to comment on variations in
504 lithospheric thickness or sublithospheric mantle structure.

Our findings indicate that the lower crust across much of the Southern African shield has a predominantly mafic composition, except for the southwest portion of the Kaapvaal Craton and western portion of the Zimbabwe Craton, where the lower crust is intermediate-to-felsic in composition. The mafic layer in the lower crust of the BC, which exceeds 15 km in thickness, is likely caused by a combination of magmatic intrusion and underplating. Both the thicker crust and the large thickness of high Vs lower crust found in the NNB, CZ, and Kheis Province are consistent with typical "suture" thickened crust found in other Precambrian terrains globally.

Most of the areas in the Kaapvaal Craton underlain by intermediate-to-felsic lower crust and a shallower Moho coincide with the region where Ventersdorp rocks have been preserved. This correlation supports the suggestion by James et al., (2003) that crustal melting during the Ventersdorp tectonomagmatic event c. 2.7 Ga could have led to extraction of a mafic component from the lower crust. Melting of the lower crust during the Ventersdorp event may not have resulted in the removal of the lower mafic crust unless it was accompanied by concomitant thinning of the crust caused by rifting. A similar explanation could be invoked for the low Vs observed in the lower crust in the western part of the Tokwe terrain, which is overlain by a 3.1 – 2.95 Ga transgressive passive margin and rift sequences. The absence of mafic xenoliths in the Kimberley terrain and the presence of mafic xenoliths in the other terrains is consistent with the variability in the shear velocity structure of the lower crust found in this study.

Acknowledgements:

We would like to thank all those who assisted with the South African Seismic Experiment. Eldridge Kgaswane would like to acknowledge support from the Council for Geoscience while working on this study. We would like to thank Mulugeta Dugda, Charles Ammon and Yongcheol Park with assistance in the software aspects of this research. This

research has been supported by the National Science Foundations (grants EAR 0440032 and OISE 0530062). Prepared by LLNL under Contract DE-AC52-07NA27344.

References

Ammon, C.J., G.E. Randall, and G. Zandt (1990), On the non-uniqueness of receiver function inversions, *Journal of Geophysical Research*, 95, 15303 – 15318.

Barton, J.M. Jr., R.E.P. Fripp, P. Horrocks, and N. McLean (1979), The geology, age and tectonic setting of the Messina Layered Intrusion, Limpopo Mobile Belt, southern Africa, *American Journal of Science*, 279, 1108 – 1134.

Berger, M., J.D. Kramers, and T.F. Nägler (1995), Geochemistry and geochronology of charno-enderbites in the Northern Marginal Zone of the Limpopo Belt, southern Africa and genetic models. *Schweiz. Mineral. Petrogr. Mitt. (Swiss Bulletin of Mineralogy and Petrology)*, 75, 17 – 42.

Berteussen, K. A., 1977. Moho depth determinations based on spectral ratio analysis, *Physics of the Earth Planetary Interiors*, 31, 313 – 326.

Black, R., R. Caby, A. Moussine-Pouchkine, J.M. Bertad, A.M. Boullier, J. Fabre, and A. Lesquer (1979), Evidence for late Precambrian plate tectonics in West Africa, *Nature*, 278, 223 – 227.

Bloch, S., A.L. Hales and M. Landisman (1969), Velocities in the crust and upper mantle of southern Africa from multi-mode surface wave dispersion, *Bulletin of the Seismological Society of America*, 59, 1599 – 1629.

Blot, C., Y. Crenn, and R. Rechenmann (1962). Elements apportes par la gravimetrie a la connaissance de la tectonique profonde du Senegal, *C.R. Acad. Sci. Paris*, 254, 1131 – 1133.

Carlson, R.W., T.L. Grove, M.J. de Wit, and J.J. Gurney (1996), Program to study the crust and mantle of the Archean Craton in southern Africa, *EOS Transactions, American Geophysical Union*, 77, 273 – 277.

560 Cassidy, J.F. (1992), Numerical experiments in broad-band receiver function analysis, *Bulletin of*
561 *Seismological Society of America*, 82, 1453 – 1474.
562
563 Christensen, N. I., and W. D. Mooney (1995), Seismic velocity structure and composition of the
564 continental crust: A global view, *Journal of Geophysical Research*, 100, no. B7, 9761 – 9788.
565
566 Cornell, D.H., R.J. Thomas, H.F.G. Moen, D.L. Reid, J.M. Moore, and R.L. Gibson (2006), The
567 Namaqua-Natal Province, *In*: M. R. Johnson, C. R. Anhaeusser, R. J. Thomas (Editors) *The Geology of*
568 *South Africa*, Geological Society of South Africa, Johannesburg/ Council for Geoscience, Pretoria, 325 –
569 379.
570
571 Cawthorn, R.G., H.V. Eales, F. Walraven, R. Uken, and M.K. Watkeys (2006), The Bushveld Complex,
572 *In*: M. R. Johnson, C. R. Anhaeusser, R. J. Thomas (Editors) *The Geology of South Africa*, Geological
573 Society of South Africa, Johannesburg/ Council for Geoscience, Pretoria, 261 – 281.
574
575 Dawson, J.B., (1980), Kimberlites and their Xenoliths, Springer-Verlag, Berlin.
576
577 Dawson, J.B., and J.V. Smith (1987), Reduced sapphirine granulite xenoliths from the Lace Kimberlite,
578 South Africa: implications for the deep structure of the Kaapvaal Craton, *Contributions to Mineralogy*
579 *and Petrology*, 95, 376 – 383.
580
581 Dawson, J.B., S.L. Harley, R.L. Rudnick, and T.R. Ireland (1997), Equilibration and reaction in Archaean
582 quartz-sapphirine granulite xenoliths from the Lace kimberlite pipe, South Africa, *Journal of*
583 *Metamorphic Geology*, 15, 253 – 266.
584
585 De Wit, M.J., C. Roering, R.J. Hart, R.A. Armstrong, C.E.J. Ronde, R.W.E. Green, M. Tredoux, E.
586 Peberdy, R.A. Hart (1992), Formation of an Archaean continent, *Nature*, 357, 553 – 562.
587
588 De Wit, M.J., and J. Tinker (2004), Crustal structures across the central Kaapvaal Craton from deep-
589 seismic reflection data, *South African Journal of Geology*, 107, 185 – 206.
590
591 Dirks, P.H.G.M. and H.A. Jelsma (2002), Crust-mantle decoupling and the growth of the Archaean
592 Zimbabwe Craton, *Journal of African Earth Sciences*, 34, 157 – 166.
593

Dugda, M.T., A.A. Nyblade, and J. Julià (2007), Thin lithosphere beneath the Ethiopian Plateau revealed by a joint inversion of Rayleigh wave group velocities and receiver functions, *Journal of Geophysical Research*, 112, B08305, doi: 10.1029/2006JB004918.

Durrheim, R.J., and R.W.E. Green (1992), A seismic refraction investigation of the Archaean Kaapvaal Craton, South Africa, using the mine tremors as the energy source, *Geophysical Journal International*, 108, 812 – 832.

Dziewonski, A.M., and D.L. Anderson (1981), Preliminary reference Earth model, *Physics of the Earth Planetary Interiors*, 25, S.297 – 356.

Eglington, B.M., and R.A. Armstrong (2004), The Kaapvaal Craton and adjacent orogens, southern Africa: a geochronological database and overview of the geological development of the Craton, *South African Journal of Geology*, 107, 13 – 32.

Gane, P.G., H.J. Logie, J.H. Stephen (1949), Triggered telerecording seismic equipment, *Bulletin of Seismological Society of America*, 39, 117 – 143.

Gane, P.G., A.R. Atkins, J.P.F. Sellschop, and P. Seligman (1956), Crustal structure in the Transvaal, *Bulletin of Seismological Society of America*, 46, 293 – 316.

Gibb, R. A., M.D. Thomas, P. Lapointe, and M. Mukhopadhay (1983), Geophysics of proposed Proterozoic sutures in Canada, *Precambrian Research*, 19, 349 – 384.

Green, R.W.E., and R.J. Durrheim (1990), A seismic refraction investigation of the Namaqualand Metamorphic Complex, South Africa, *Journal of Geophysical Research*, 95, No. B12, 19927 – 19932.

Gurrola, H., and J.B. Minster (1998), Thickness estimates of the upper-mantle transition zone from bootstrapped velocity spectrum stacks of receiver functions, *Geophysical Journal International*, 133, 31 – 43.

Hales, A.L., and I.S. Sacks (1959), Evidence for an intermediate layer from crustal structure studies in the eastern Transvaal, *Geophysical Journal of the Royal Astronomical Society*, 2, 15 – 33.

Harvey, J.D., M.J. de Wit, J. Stankiewicz, and C.M. Doucouré (2001), Structural variations of the crust in the Southwestern Cape, deduced from seismic receiver functions, *South African Journal of Geology*, 104, 231 – 242.

Hatton, C.J. and J.K. Schweitzer (1995), Evidence for synchronous extrusive and intrusive Bushveld magmatism, *Journal of African Earth Sciences*, 21, 579 – 594.

Holbrook, W.S., W.D. Mooney and N.I. Christensen (1992), The seismic velocity structure of the deep continental crust, Chapter 1, *In*: D. M. Fountain, R. Arculus and R. W. Kay (Editors), *Continental Lower Crust*, 1 – 43.

James, D.E., F. Niu, and J. Rokosky (2003), Crustal structure of the Kaapvaal Craton and its significance for early crustal evolution. *Lithos*, 71, 413 – 429.

Jelsma, H. A. and P.H.G.M. Dirks (2002), Neoarchaean tectonic evolution of the Zimbabwe Craton. In C.M.R. Fowler, C.J. Ebinger and C.J. Hawkesworth (Editors), *The Early Earth: Physical, Chemical and Biological Development. Geological Society of London, Special Publications,* 199*,* 183 – 211.

Johnson, M.R., C.R. Anhaeusser, and R.J. Thomas (Editors) (2006). *The Geology of South Africa*. Geological Society of South Africa, Johannesburg/ Council for Geoscience, Pretoria, 691 pp.

Julià, J., C.J. Ammon, R.B. Hermann, and A.M. Correig (2000), Joint inversion of receiver functions and surface-wave dispersion observations. *Geophysical Journal International*, 143, 99 – 112.

Julià, J., C.J. Ammon, and R.B. Hermann (2003), Lithospheric structure of the Arabian Shield from the joint inversion of receiver functions and surface-wave group velocities, *Tectonophysics*, 371, 1 – 21.

Julià, J., C.J. Ammon, and A.A. Nyblade (2005), Evidence for mafic lower crust in Tanzania, East Africa from joint inversion of receiver functions and Rayleigh wave dispersion velocities, *Geophysical Journal International*, 162, 555 – 569.

Julià, J. (2007), Constraining velocity and density contrasts across the crust-mantle boundary with receiver function amplitudes, *Geophysical Journal International*, 171, 286 – 301.

662 Kramers, J.D., S. McCourt and D.D. van Reenen (2006), The Limpopo Belt, *In*: M. R. Johnson, C. R.
663 Anhaeusser, R. J. Thomas (Editors) *The Geology of South Africa*, Geological Society of South Africa,
664 Johannesburg/ Council for Geoscience, Pretoria, 209 – 236.
665
666 Kreissig, K., Th. F. Nägler, J.D. Kramers, D.D. Van Reenen, and C.A. Smit (2000), An isotopic and
667 geochemical study of the northern Kaapvaal Craton and the Southern Marginal Zone of the Limpopo
668 Belt: are they juxtaposed terrains? *Lithos*, 50, 1 – 25.
669
670 Kwadiba, M.T.O.G., C. Wright, E.M. Kgaswane, R.E. Simon, and T.K. Nguuri (2003), Pn arrivals and
671 lateral variations of Moho geometry beneath the Kaapvaal Craton, *Lithos*, 71, 393– 411.
672
673 Langston, C.A. (1979), Structure under Mount Rainier, Washington, inferred from teleseismic body
674 waves. *Journal of Geophysical Research*, 84, 4749 – 4762.
675
676 Larson, E.W.F. and G. Ekström (2001), Global models of surface wave group velocity, *Pure and Applied*
677 *Geophysics*, 158, no. 8, 1377 – 1400.
678
679 Li, A., and K. Burke (2006), Upper mantle structure of southern Africa from Rayleigh wave tomography,
680 *Journal of Geophysical Research*, 111, B10303, doi:10.1029/2006JB004321.
681
682 Ligorría, J.P., and C. J. Ammon (1999), Iterative deconvolution and receiver function estimation, *Bulletin*
683 *of Seismological Society of America*, 89, 1359 – 1400.
684
685 Louis, P. (1978), Gravimetrie et geologie en Afrique occidentale et centrale, *Mem. Bur. Rech. Geol. Min.*,
686 91, 53 – 61.
687
688 Mathur, S.P. (1974), Crustal structure in southwestern Australia from seismic and gravity data,
689 *Tectonophysics*, 24, 151 – 182.
690
691 McCourt, S. and R.A. Armstrong (1998), SIMS U-Pb zircon geochronology of granites from the Central
692 Zone, Limpopo Belt, southern Africa: implications for the age of the Limpopo Orogeny, *South African*
693 *Journal of Geology*, 101, 329 – 338.
694
695 McCourt, S., P. Hilliard, R.A. Armstrong, and H. Munyanyiwa (2001). Shrimp U-Pb zircon
696 geochronology of the Hurungwe granite northwest Zimbabwe: Age constraints on the timing of the

Magondi orogeny and implications for the correlation between the Kheis and Magondi Belts, *South African Journal of Geology*, 104, 39 – 46.

Moen, H.F.G. (1999), The Kheis Tectonic Subprovince, southern Africa: a lithostratigraphic perspective, *South African Journal of Geology*, 102, 27 – 42.

Nair, S.K., S.S. Gao, H.L. Kelly, and P.G. Silver (2006), Southern African crustal evolution and composition: Constraints from receiver function studies, *Journal of Geophysical Research*, 111, B02304, doi:10.1029/2005JB003802.

Newton, A.R., R.W. Shone, and P.W.K. Booth (2006), The Cape Fold Belt, *In*: M. R. Johnson, C. R. Anhaeusser, R. J. Thomas (Editors) *The Geology of South Africa*, Geological Society of South Africa, Johannesburg/ Council for Geoscience, Pretoria, 521 – 530.

Nixon, P. H., (1987), Kimberlitic xenoliths and their cratonic setting, *In*: P. H. Nixon (Editor) Mantle Xenoliths, John Wiley and Sons Ltd., 215 – 239.

Nguuri, T.K., J. Gore, D.E. James, S. J. Webb, C. Wright, T.G. Zengeni, O. Gwavava, J.A. Snoke, and Kaapvaal Seismic Group (2001), Crustal structure beneath southern africa and its implications for the formation and evolution of the Kaapvaal and Zimbabwe Cratons, *Geophysical Research Letters, 28*, 13, 2501 – 2504.

Nguuri, T., (2004), Crustal structure of the Kaapvaal Craton and surrounding mobile belts: analysis of teleseismic P waveforms and surface wave inversions, Ph.D. dissertation, University of the Witwatersrand (unpublished).

Niu, F., and D.E. James (2002), Fine structure of the lowermost crust beneath the Kaapvaal Craton and its implications for crustal formation and evolution, *Earth and Planetary Science Letters*, 200, 121 – 130.

Nyblade, A.A., and H.N. Pollack (1992), A gravity model for the lithosphere in western Kenya and northeastern Tanzania, *Tectonophysics*, 212, 257 – 267.

Owens, T.J., and G. Zandt (1985), The response of the continental crust-mantle boundary observed on broadband teleseismic receiver functions, *Geophysical Research Letters*, 14, 824 – 827.

732 Pasyanos, M.E., and A.A. Nyblade (2007), A top to bottom lithospheric study of Africa and Arabia,
733 *Tectonophysics*, 444, no. 1 – 4, 27 – 44.
734
735 Pretorius, W., and J. M. Barton, Jr, (2003), Measured and calculated compressional wave velocities of
736 crustal and upper mantle rocks in the Central Zone of the Limpopo Belt, South Africa – implications for
737 lithospheric structure, *South African Journal of Geology*, 106, 205 – 212.
738
739 Qiu, X., K. Priestley, and D. McKenzie (1996), Average lithospheric structure of southern Africa,
740 *Geophysical Journal International*, 127, no. 3, 563 – 581.
741
742 Ransome, I.G.D. and M.J. de Wit (1992), Preliminary investigations into a microplate model for the
743 South Western Cape. In: De Wit, M.J. and Ransome, I.G.D. (Eds.), *Inversion Tectonics of the Cape Fold*
744 *Belt, Karoo and Cretaceous Basins of Southern Africa*. A.A. Balkema, Rotterdam, 257 – 266.
745
746 Rudnick, R.L., and D.M. Fountain (1995), Nature and composition of the continental crust: a lower crust
747 perpective, *Reviews of Geophysics*, 33, 3, 267 – 309.
748
749 Rudnick, R.L., and S. Gao (2003), Treatise on Geochemistry, vol. 3, 1 – 64.
750
751 SACS (South African Committee for Stratigraphy) (1980), Stratigraphy of South Africa. Part 1 (Kent,
752 L.E., Comp.), Lithostratigraphy of the Republic of South Africa, South West Africa/Namibia, and the
753 Republics of Bophuthatswana, Transkei and Venda. *Handbook of Geological Survey of South Africa, 8,*
754 *690 pp*.
755
756 Schmitz, M.D., and S.A. Bowring (2003a), Constraints on the thermal evolution of continental
757 lithosphere from U-Pb accessory mineral thermochronometry of lower crustal xenoliths, southern Africa,
758 *Contributions to Mineralogy and Petrology*, 144, 592 – 618.
759
760 Schmitz, M.D., and S.A. Bowring (2003b), Ultrahigh-temperature metamorphism in the lower crust
761 during Neoarchean Ventersdorp rifting and magmatism, Kaapvaal Craton, southern Africa, *Geological*
762 *Society of America Bulletin*, 115, 533 – 548.
763
764 Simon, R.E., C. Wright, E.M. Kgaswane, and M.T.O. Kwadiba (2002). The P wavespeed structure below
765 and around the Kaapvaal Craton to depths of 800 km, from traveltimes and waveforms of local and
766 regional earthquakes and mining-induced tremors, *Geophysical Journal International*, 151, 132 – 145.

Stankiewicz, J., S. Chevrot, R.D. van der Hilst, and M.J. de Wit (2002), Crustal thickness, discontinuity depth, and upper mantle structure beneath southern Africa: constraints from body wave conversions, *Physics of the Earth and Planetary Interiors*, 130, 235 – 251.

Stowe, C.W. (1986), Synthesis and interpretation of structures along the north-eastern boundary of the Namaqua Tectonic Province, South Africa, *Transactions of the Geological Society of South Africa*, 89, 185 – 198.

Stowe, C.W. (1989), Discussion on 'The Proterozoic Magondi Belt in Zimbabwe – a review', *South African Journal of Geology*, 92, 69 – 71.

Subrahmanyam, C. (1978), On the relation of gravity anomalies to geotectonics of the Precambrian terrains of the south Indian shield, *Journal of Geological Society of India*, 19, 251 – 263.

Thamm, A. G., and M. R. Johnson (2006), The Cape Supergroup, *In*: M. R. Johnson, C. R. Anhaeusser, R. J. Thomas (Editors) *The Geology of South Africa*, Geological Society of South Africa, Johannesburg/ Council for Geoscience, Pretoria, 443 – 460.

Van der Westhuizen, W.A., H. de Bruiyn, and P.G. Meintjes (2006), The Ventersdorp Supergroup, *In*: M. R. Johnson, C. R. Anhaeusser, R. J. Thomas (Editors) *The Geology of South Africa*, Geological Society of South Africa, Johannesburg/ Council for Geoscience, Pretoria, 187 – 208.

Von Gruenewaldt, G., M.R. Sharpe, and C.J. Hatton (1985), The Bushveld Complex; introduction and review, *Economic Geology*, 80, 803 – 812.

Webb, S.J., R.G. Cawthorn, T.K. Nguuri, and D.E. James (2004), Gravity modelling of Bushveld Complex connectivity supported by Southern African Seismic Experiment results, *South African Journal of Geology*, 107, 207 – 218.

Wellmann, P. (1978), Gravity evidence for abrupt changes in the mean crustal density at the junction of Australian crustal blocks, *Aust. Bur. Miner. Resour. Geol. Geophys. Bull.*, 3, 153 – 162.

Willmore, P.L., A.L. Hales, and P.G. Gane (1952), A seismic investigation of crustal structure in the western Transvaal, *Bulletin of Seismological Society of America*, 42, 53 – 80.

Wright, C., E.M. Kgaswane, M.T.O. Kwadiba,, R.E. Simon, T.K. Nguuri, and R. McRae-Samuel (2003), South African seismicity, April 1997 – April 1999, and regional variations in the crust and uppermost mantle of the Kaapvaal Craton, *Lithos*, 71, 369 – 392.

Zhao, M., C.A. Langston, A.A. Nyblade, and T.J. Owens (1999), Upper mantle velocity structure beneath southern Africa from modelling regional data, *Journal of Geophysical Research*, 104, no. B3, 4783 – 4794.

827 # Tables

828

829 **Table 1.** Average Vp/Vs ratios of the geological terrains in southern Africa

	Kaapvaal Craton		Zimbabwe Craton		Bushveld Complex		Namaqua-Natal Belt		Limpopo Belt		Kheis terrain	
	Vp/Vs	**#s**	**Vp/Vs**	**#s**	**Vp/Vs**	**#s**	**Vp/Vs**	**#s**	**Vp/Vs**	**#s**	**Vp/Vs**	**#s**
Nguuri (2004)	1.72 ± 0.05	35	-	-	1.79 ± 0.06	14	1.78 ± 0.05	10	1.84 ± 0.06	12	1.74 ± 0.06	4
Nair et al (2006)	1.74 ± 0.01	25	1.73 ± 0.01	5	1.78 ± 0.02	5	1.72 ± 0.01	5	1.74 ± 0.01	4	1.73 ± 0.01	4

830 **#s = Number of stations**

Table 2. Summary of crustal structure by terrain

	Terrain	Average Moho depth ± standard deviation (km)	Number of stations	Sn (km/s)	Average Vs of the crust ± standard deviation (km)	Average Vs below 20 km depth (km/s)	Average Vs below 30 km depth (km/s)	Average thickness of layers with Vs ≥ 4.0 km/s (km)
Kaapvaal Craton	**Witwatersrand**	42 ± 3	11	4.6	3.7 ± 0.1	3.9	4.0	12
	Swaziland	41± 2	4	4.7	3.7 ± 0.1	4.1	4.2	22
	Pietersburg	41 ± 2	4	4.6	3.7 ± 0.1	4.0	4.0	14
	Kimberley							
	Kimberley (central)	36 ± 1	16	4.6	3.6 ± 0.1	3.8	3.8	2
	Kimberley (N and S margins)	39 ± 1	4	4.6	3.7 ± 0.1	3.9	4.0	6
Zimbabwe Craton	**Western part of the Tokwe terrain**	37 ± 1	3	4.5	3.7 ± 0.0	3.9	3.9	4
	Eastern part of the Tokwe terrain	39 ± 3	4	4.5	3.8 ± 0.0	4.0	4.0	15
Bushveld Complex		45 ± 5	13	4.6	3.7 ± 0.1	4.0	4.1	15

Namaqua-Natal Belt		45 ± 4	7	4.8	3.9 ± 0.1	4.2	4.3	22
Limpopo Belt	**SMZ**	40 ± 0	1	4.5	3.7 ± 0.0	4.0	4.0	17
	CZ	46 ± 5	11	4.6	3.8 ± 0.0	4.0	4.1	20
	NMZ	43± 0	1	4.6	3.7 ± 0.0	4.1	4.1	23
Kheis Province		42 ± 5	7	4.5	3.8 ± 0.1	4.0	4.2	13
Okwa terrain		43± 0	1	4.5	3.7 ± 0.0	3.9	4.0	11
Cape Fold Belt		35 ± 2	2	4.7	3.8 ± 0.1	4.2	4.4	19

Figures

1. Tectonic map of southern Africa showing major Precambrian terrains. The terrain names and boundaries for South Africa are based on Eglington and Armstrong (2004). Terrain names and boundaries for the Zimbabwe Craton are based on Jelsma and Dirks (2002). Political boundaries are shown with dashed lines. PSZ – Palala Shear Zone and TML – Thabazimbi Murchison Lineament.
2. Map showing distribution of broadband seismic stations used in this study in relation to the terrain boundaries shown in Figure 1. The open square in the central part of the Kimberley terrain shows the location of the Kimberley array.
3. Distribution of teleseismic earthquakes used for this study (small solid circles). The triangle shows the centre of the SASE network. Large circles show distance in 20° increments from the centre of the network.
4. Velocity models for station SA40 obtained from the joint inversion using five different starting models. The figure illustrates that our inversion results are not sensitive to our choice of starting model.
5. Diagram for station SA55 to illustrate the procedure used for determining structure below 200 km. The four columns show different models tested for structure below 200 km depth using velocities from PREM and 2%, 3% and 5% less-than-PREM. (a) Observed (black line) and predicted (gray line) group velocity curves. The inset figures show the fit to the longest period (140 – 175 sec) group velocities for the four different models tested. (b) Observed (black line) and predicted (gray line) receiver functions. (c) The shear wave velocity models obtained from the joint inversion (black line) and the PREM shear wave velocity model (gray line) for reference. The 3% less-than-PREM model for shear wave velocities below 200 km depth gives the best fit to the longest period group velocities.

6. Error analysis of the joint inversion results using two stations, BOSA and SUR, with different lower crustal velocities. (a). Joint inversion results with lower crustal velocities constrained to 4.0 and 3.8 km/s in the starting models of BOSA and SUR, respectively. (b) 1-σ error bounds (gray shading) around the average observed receiver functions (black line) and the predicted receiver functions (dashed black line). The high (hf1, hf2) and low (lf1, lf2) frequency receiver functions are grouped in different ray parameter bins. (c) Observed group velocities plotted together with predicted group velocities. The inset figures show the same plots but highlight the differences in the observed and predicted group velocities for periods of 10 – 60 sec.
7. Comparison of crustal thickness estimates from this study with crustal thickness estimates from previous studies. The dashed line shows the 1-to-1 correlation and the solid symbols show stations that do not fall close to the 1-to-1 line.
8. Shear wave velocity profiles grouped by tectonic terrain. Moho depths are shown with horizontal lines and numbers in km. Lower crustal layers with Vs ≥ 4.0 km/s are shaded.
9. Map showing the average Vs below 30 km (gray shading) and the average layer thicknesses with Vs ≥ 4.0 km/s (shown as open and solid squares and denoted as "Th") for 1 x 1 degree blocks. The blocks without symbols are areas where the average layer thicknesses with Vs ≥ 4.0 km/s are between 5 and 15 km. Solid lines show the outlines of the tectonic terrains from Figure 1.
10. Average Vs below 30 km depth plotted against crustal thickness. The dashed lines are the linear regressions for stations with crustal thicknesses less than and greater than 40 km.
11. Figure illustrating features in the data that give rise to the difference in lower crustal structure. (a) Shear wave models obtained from the joint inversion for SA81 (Namaqua-Natal Belt, NNB) and station BOSA (Kimberley Terrain, KT). (b) Receiver functions. (c) Rayleigh group velocities.

12. Map showing distribution of the Ventersdorp supergroup (white line) taken from van der Westhuizen et al. (2006) and location of lower crust xenoliths obtained from Pretorius and Barton (2003) and Schmitz and Bowring (2003a). The numbers labels 1 -14 represent the names of the kimberlites. 1. Newlands, 2. Markt, 3. Uintjiesberg, 4. Klipfontein-08 5. Beyersfontein, 6. Lovedale, 7. Star Mine, 8. Kaalvallei, 9. Lace, 10. Voorspoed, 11. Mothae, 12. Letseng-la-Terae, 13. Matsoku, 14. Venetia Mine and 15. Jwaneng

Figure 1

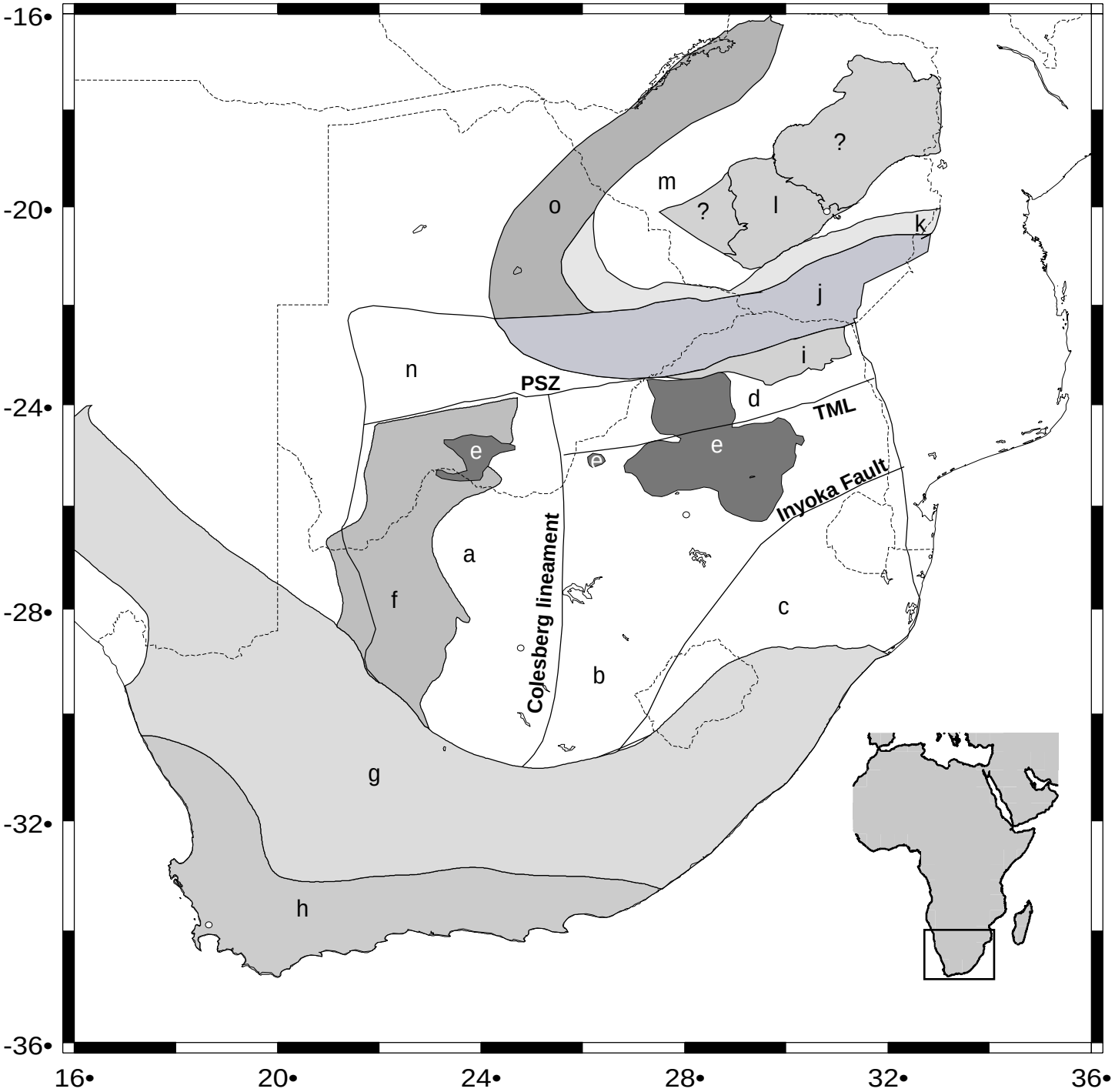

Kaapvaal Craton
- *a. Kimberley terrain*
- *b. Witwatersrand terrain*
- *c. Swaziland terrain*
- *d. Pietersburg terrain*
- *e. Bushveld Complex*

- *f. Kheis Province*
- *g. Namaqua-Natal Belt*
- *h. Cape Fold Belt*

Limpopo Belt
- *i. Southern Marginal Zone*
- *j. Central Zone*
- *k. Northern Marginal Zone*

Zimbabwe Craton
- *l. Tokwe terrain*
- *m. Granite greenstones*

- *n. Okwa terrain*
- *o. Magondi Belt*

Figure 2

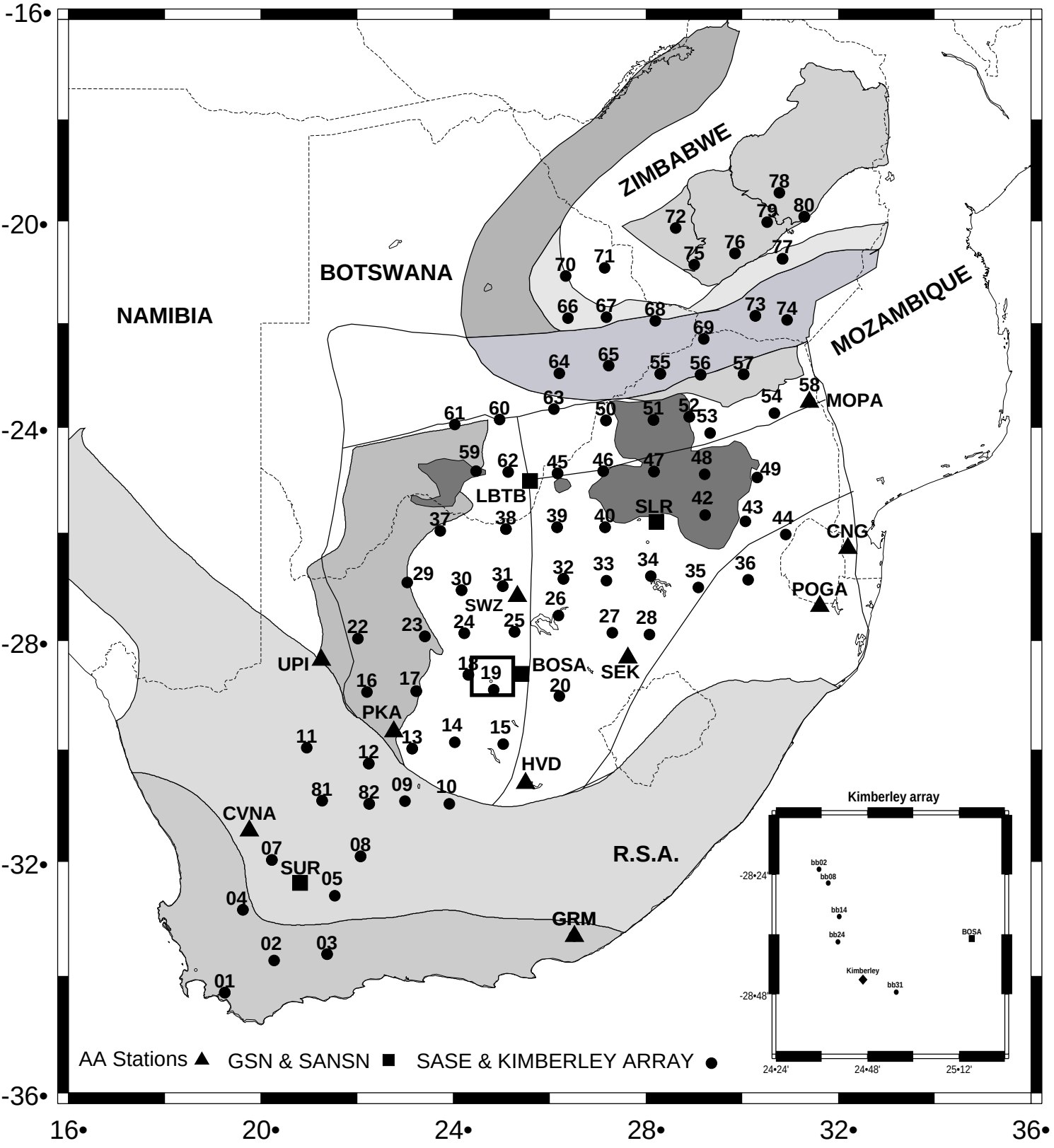
-16•
-20•
-24•
-28•
-32•
-36•
16•
20•
24•
28•
32•
36•
ZIMBABWE
BOTSWANA
NAMIBIA
MOZAMBIQUE
R.S.A.
LBTB
SLR
BOSA
SWZ
UPI
PKA
CVNA
SUR
GRM
HVD
SEK
MOPA
CNG
POGA
01
02
03
04
05
07
08
09
10
11
12
13
14
15
16
17
18
19
20
22
23
24
25
26
27
28
29
30
31
32
33
34
35
36
37
38
39
40
42
43
44
45
46
47
48
49
50
51
52
53
54
55
56
57
58
59
60
61
62
63
64
65
66
67
68
69
70
71
72
73
74
75
76
77
78
79
80
81
82
Kimberley array
bb02
bb08
bb14
bb24
BOSA
Kimberley
bb31
-28•24'
-28•48'
24•24'
24•48'
25•12'
AA Stations ▲ GSN & SANSN ■ SASE & KIMBERLEY ARRAY ●

Figure 3

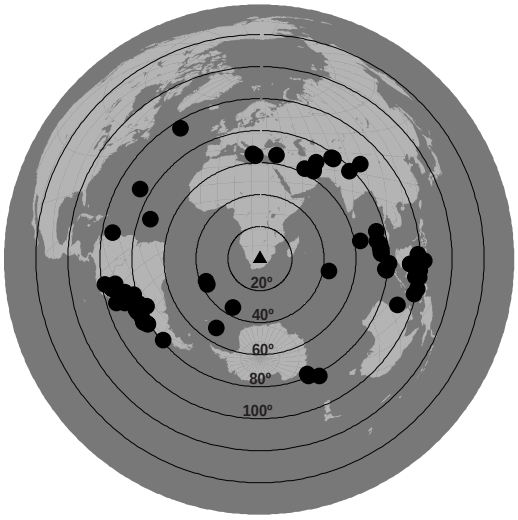

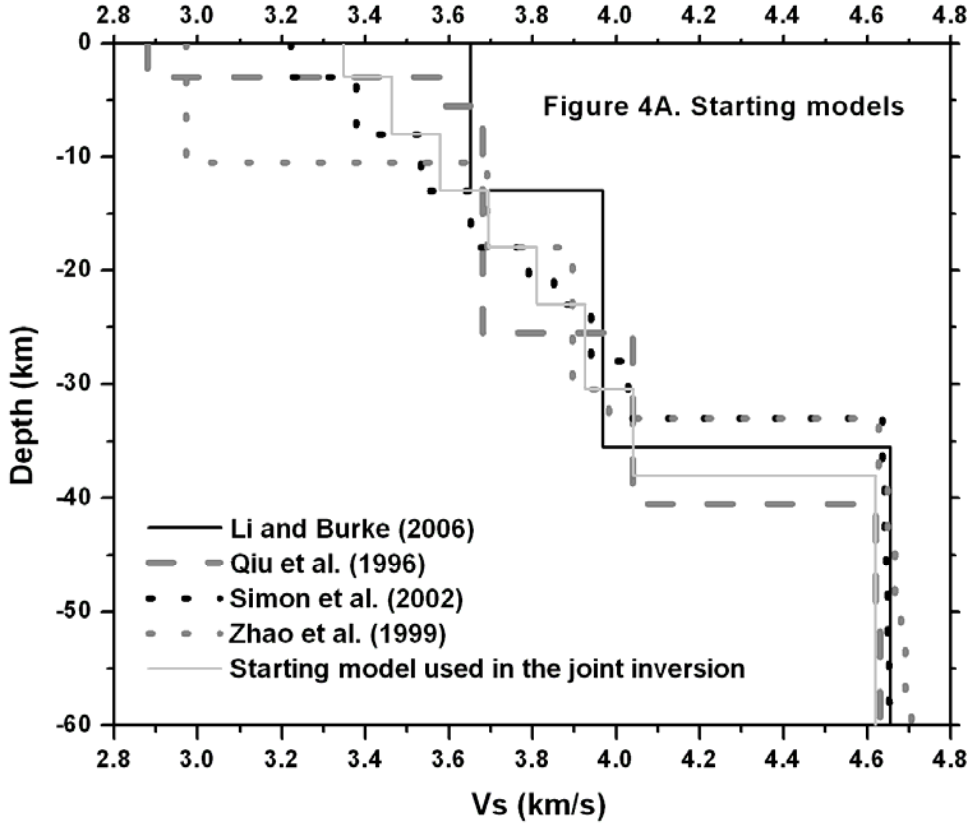
Figure 4A. Starting models
Depth (km)
Vs (km/s)
Li and Burke (2006)
Qiu et al. (1996)
Simon et al. (2002)
Zhao et al. (1999)
Starting model used in the joint inversion

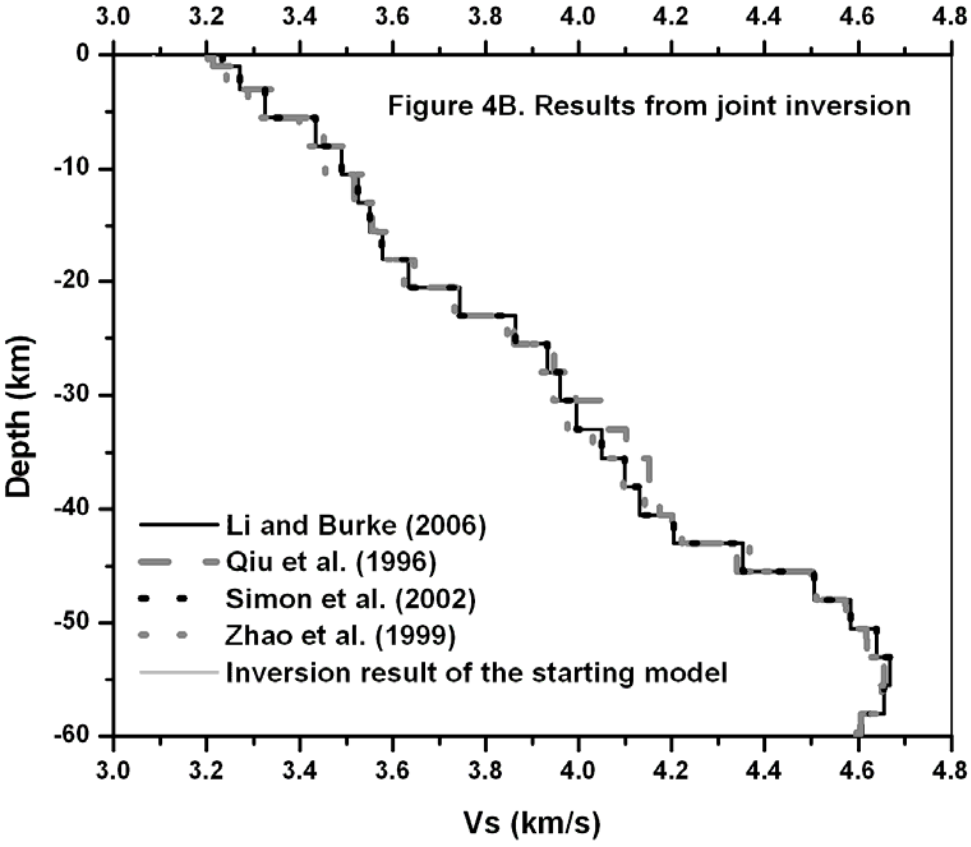
Figure 4B. Results from joint inversion
Depth (km)
Vs (km/s)
Li and Burke (2006)
Qiu et al. (1996)
Simon et al. (2002)
Zhao et al. (1999)
Inversion result of the starting model

Figure 5

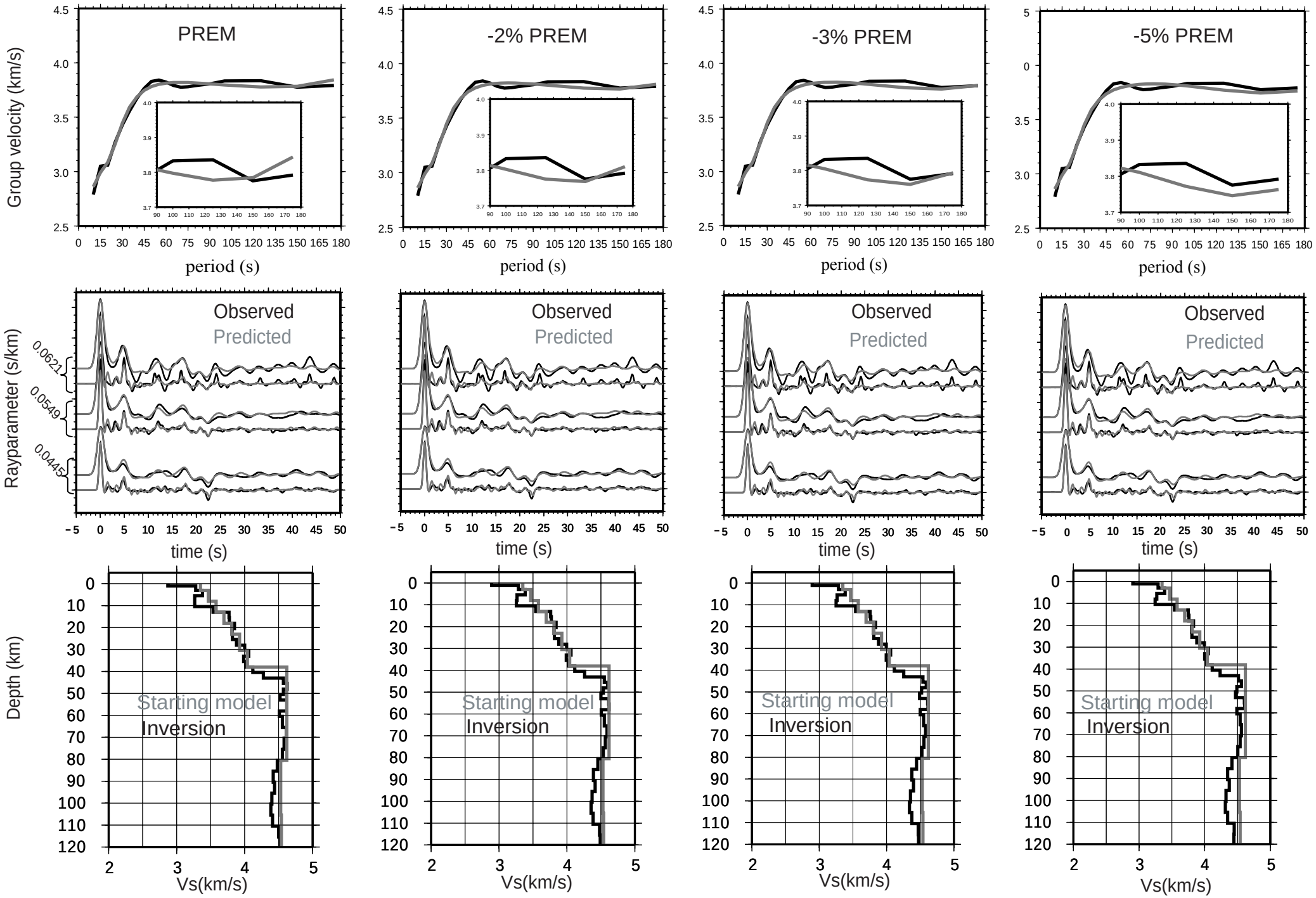
PREM
-2% PREM
-3% PREM
-5% PREM
Group velocity (km/s)
period (s)
Observed
Predicted
Rayparameter (s/km)
0.0621
0.0549
0.0445
time (s)
Depth (km)
Starting model
Inversion
Vs(km/s)

Figure 6

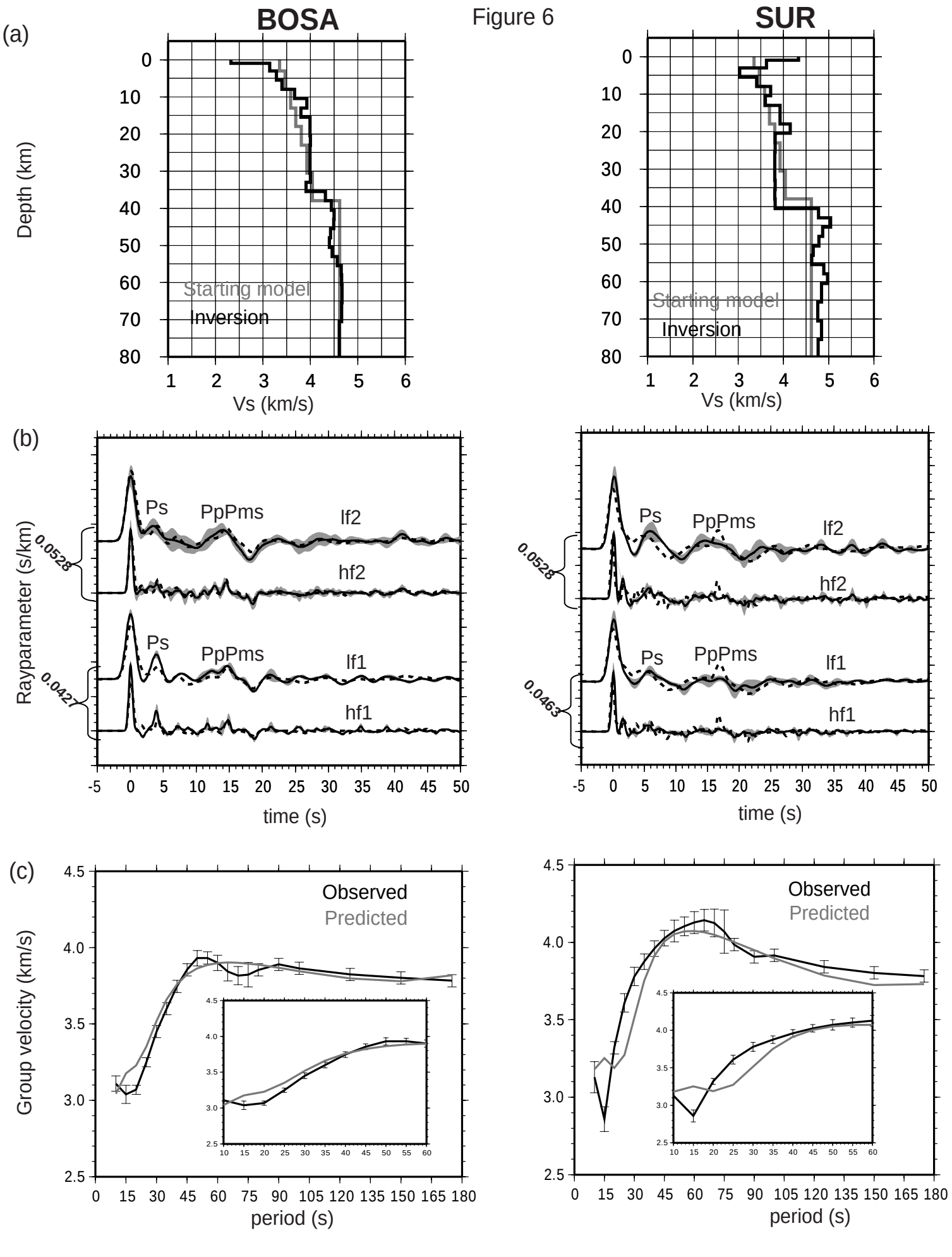
(a)
BOSA
SUR
Depth (km)
Vs (km/s)
Starting model
Inversion
(b)
Rayparameter (s/km)
0.0528
0.0427
0.0463
Ps
PpPms
lf2
hf2
lf1
hf1
time (s)
(c)
Group velocity (km/s)
Observed
Predicted
period (s)

Figure 7

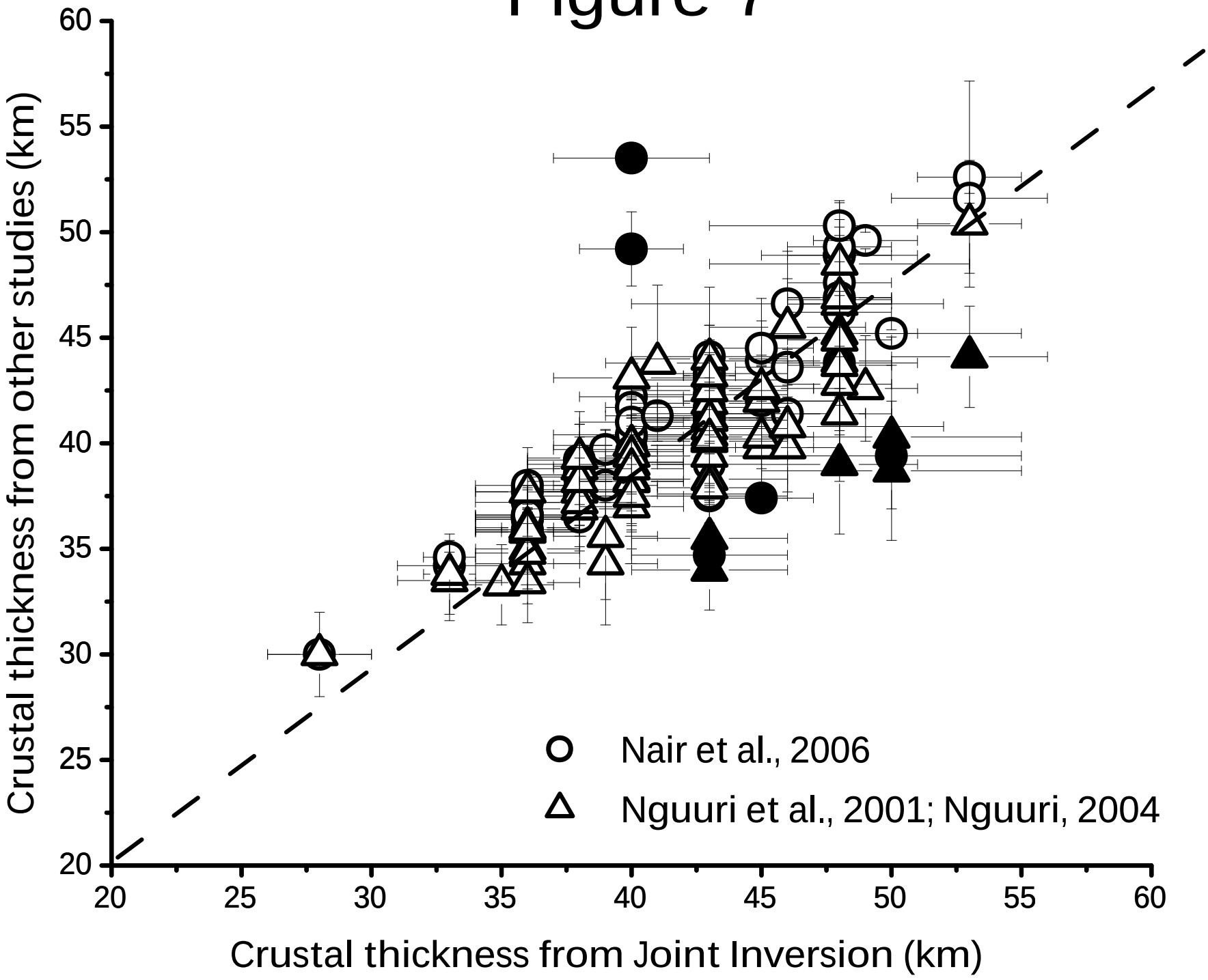
Crustal thickness from other studies (km)
Crustal thickness from Joint Inversion (km)
20
25
30
35
40
45
50
55
60
Nair et al., 2006
Nguuri et al., 2001; Nguuri, 2004

Figure 8a

Kaapvaal and Zimbabwe craton

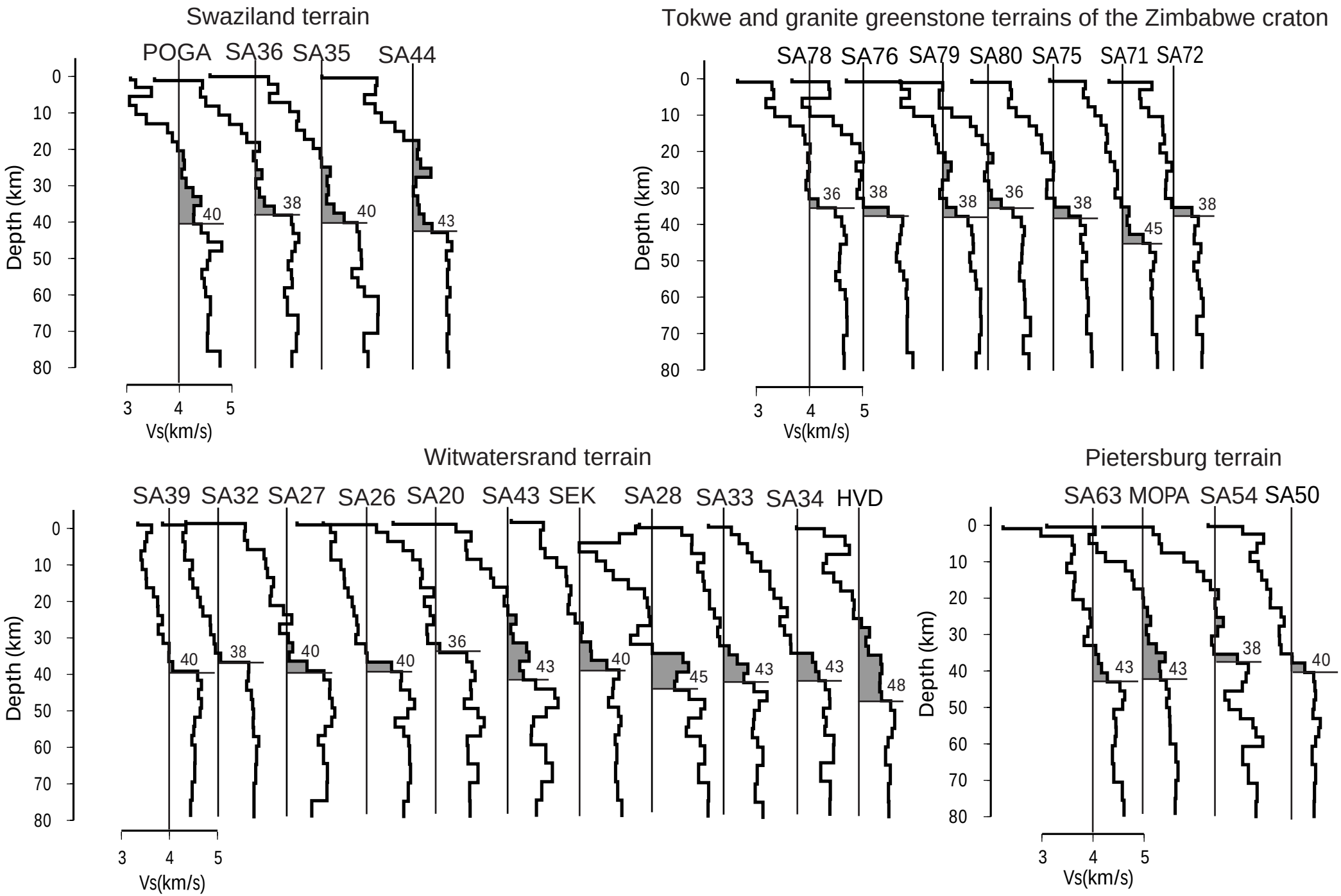

Figure 8b

Kaapvaal craton- Kimberley terrain

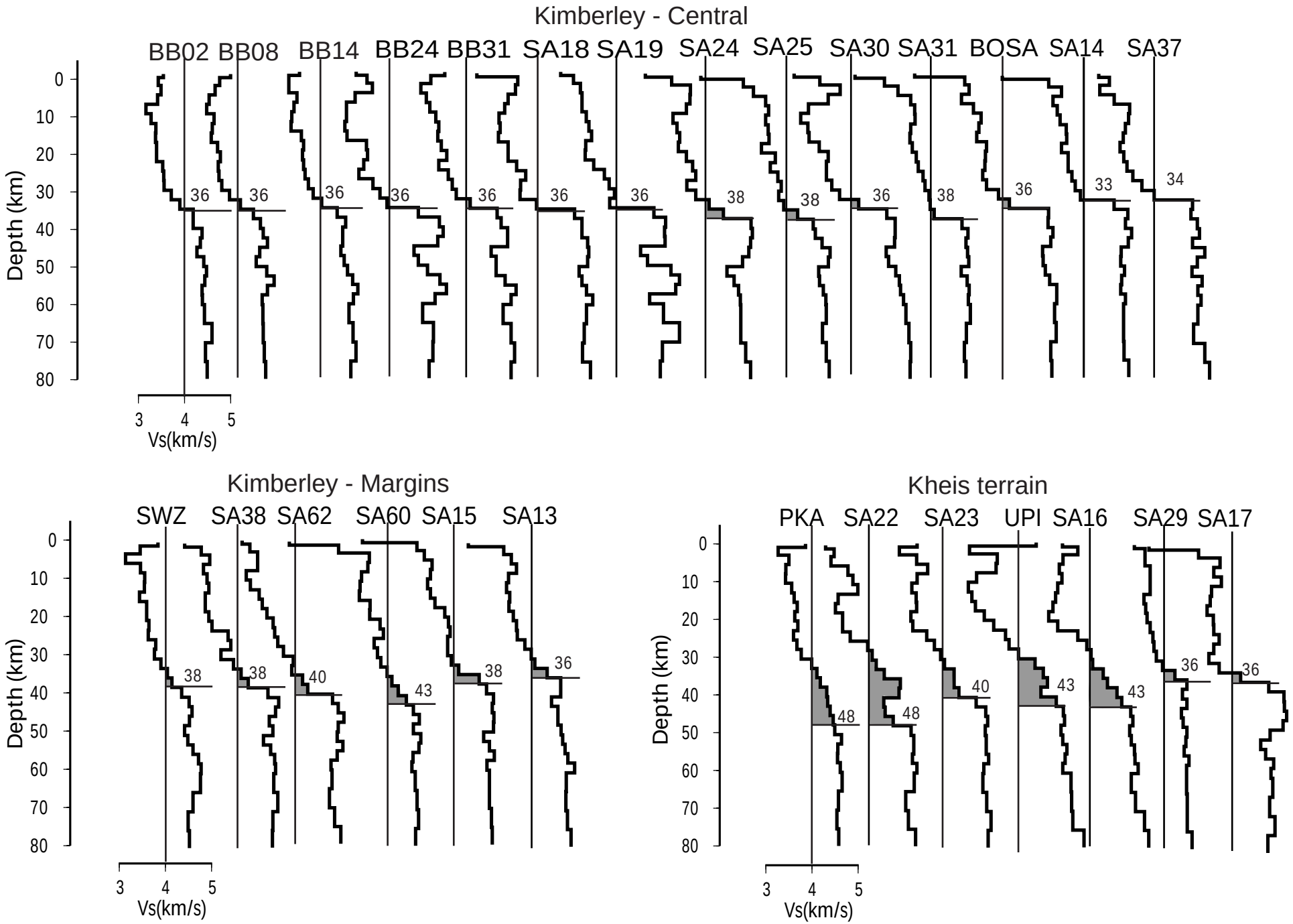

Figure 8c

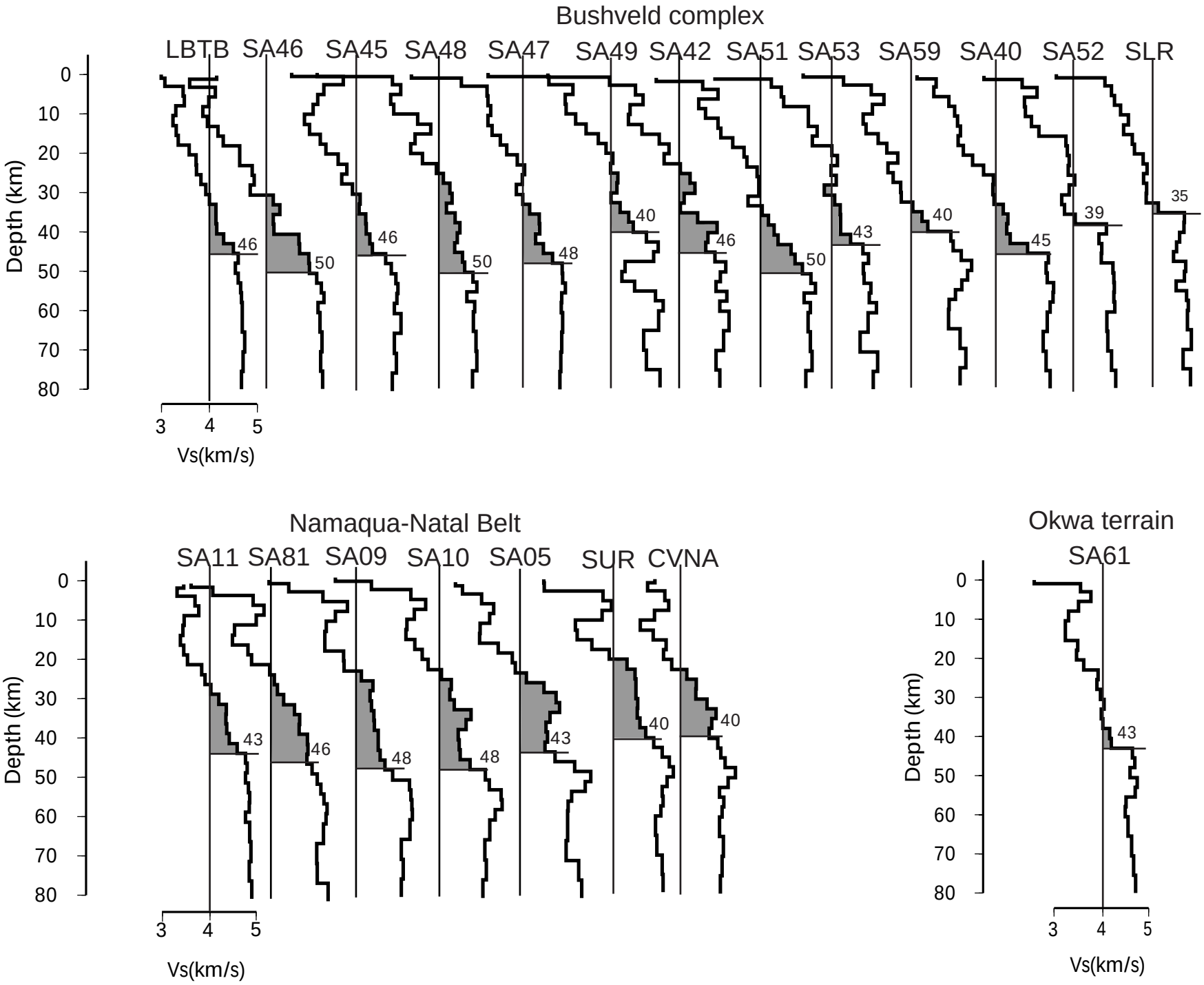
Bushveld complex
LBTB
SA46
SA45
SA48
SA47
SA49
SA42
SA51
SA53
SA59
SA40
SA52
SLR
Depth (km)
0
10
20
30
40
50
60
70
80
46
50
46
50
48
40
46
50
43
40
45
39
35
3
4
5
Vs(km/s)
Namaqua-Natal Belt
SA11
SA81
SA09
SA10
SA05
SUR
CVNA
43
46
48
48
43
40
40
Okwa terrain
SA61
43

Figure 8d

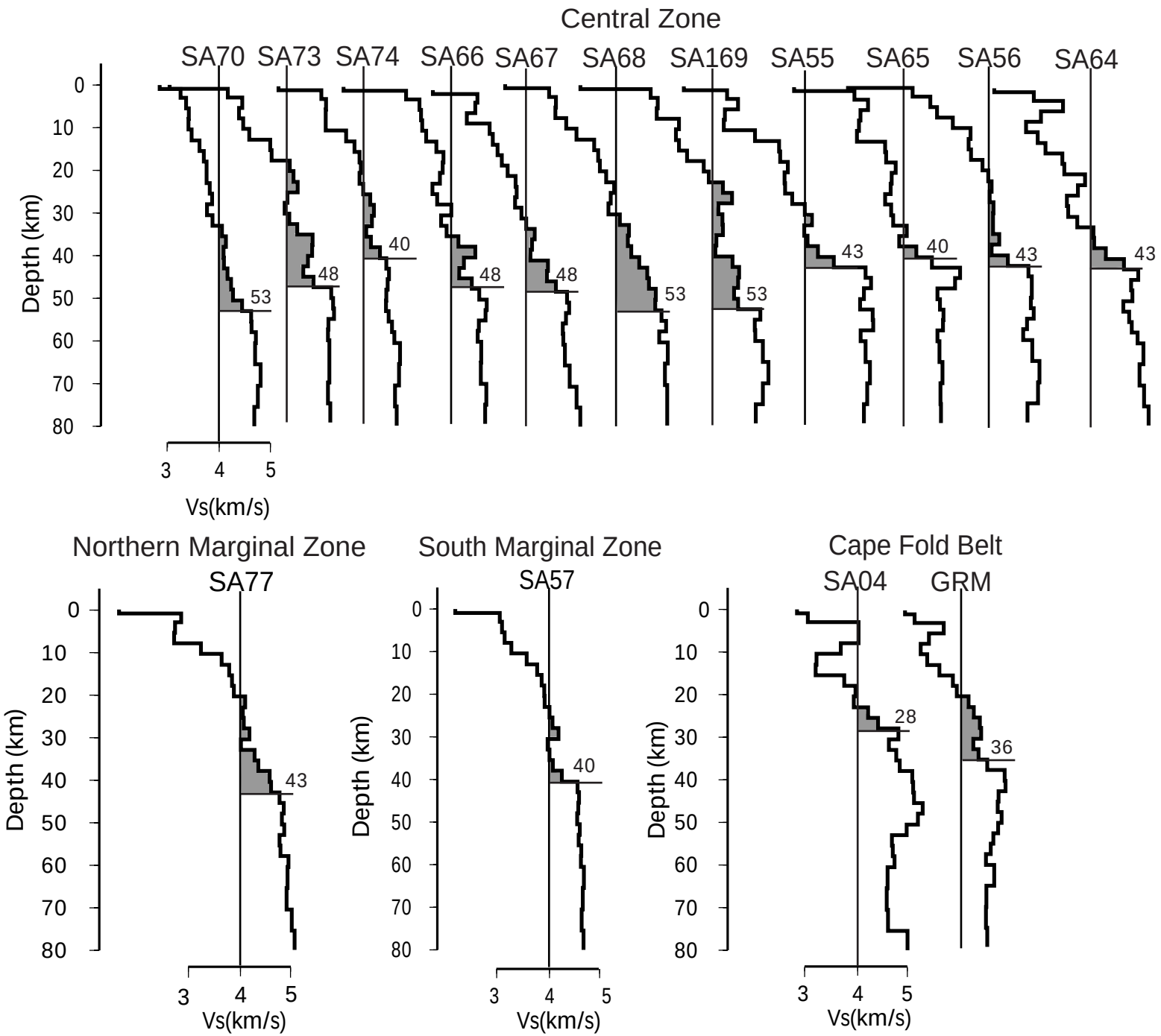
Limpopo Belt
Central Zone
SA70
SA73
SA74
SA66
SA67
SA68
SA169
SA55
SA65
SA56
SA64
Depth (km)
0
10
20
30
40
50
60
70
80
53
48
40
48
48
53
53
43
40
43
43
3
4
5
Vs(km/s)
Northern Marginal Zone
SA77
43
South Marginal Zone
SA57
40
Cape Fold Belt
SA04
GRM
28
36

Figure 9

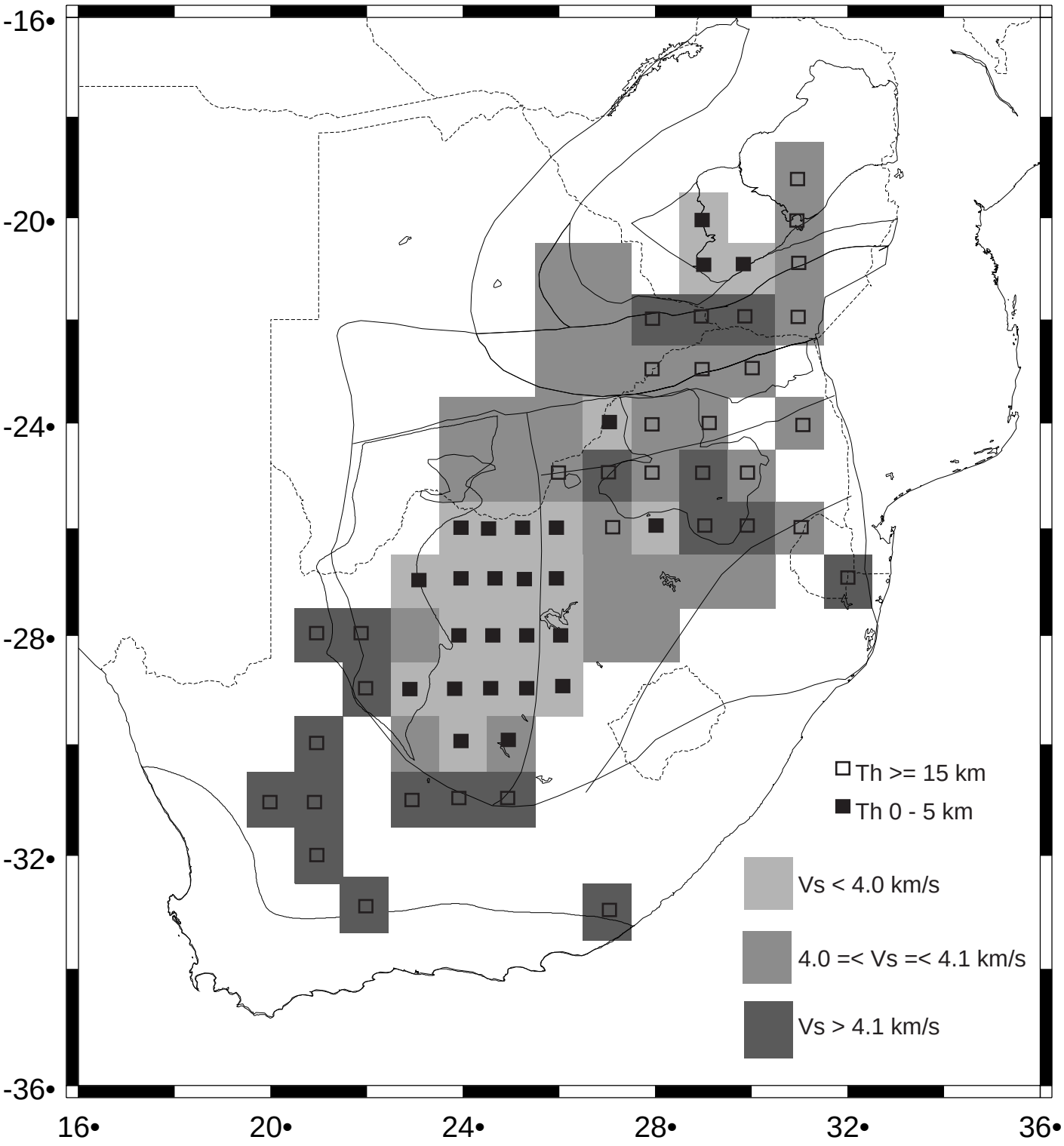
-16•
-20•
-24•
-28•
-32•
-36•
16•
20•
24•
28•
32•
36•
Th >= 15 km
Th 0 - 5 km
Vs < 4.0 km/s
4.0 =< Vs =< 4.1 km/s
Vs > 4.1 km/s

Figure 10

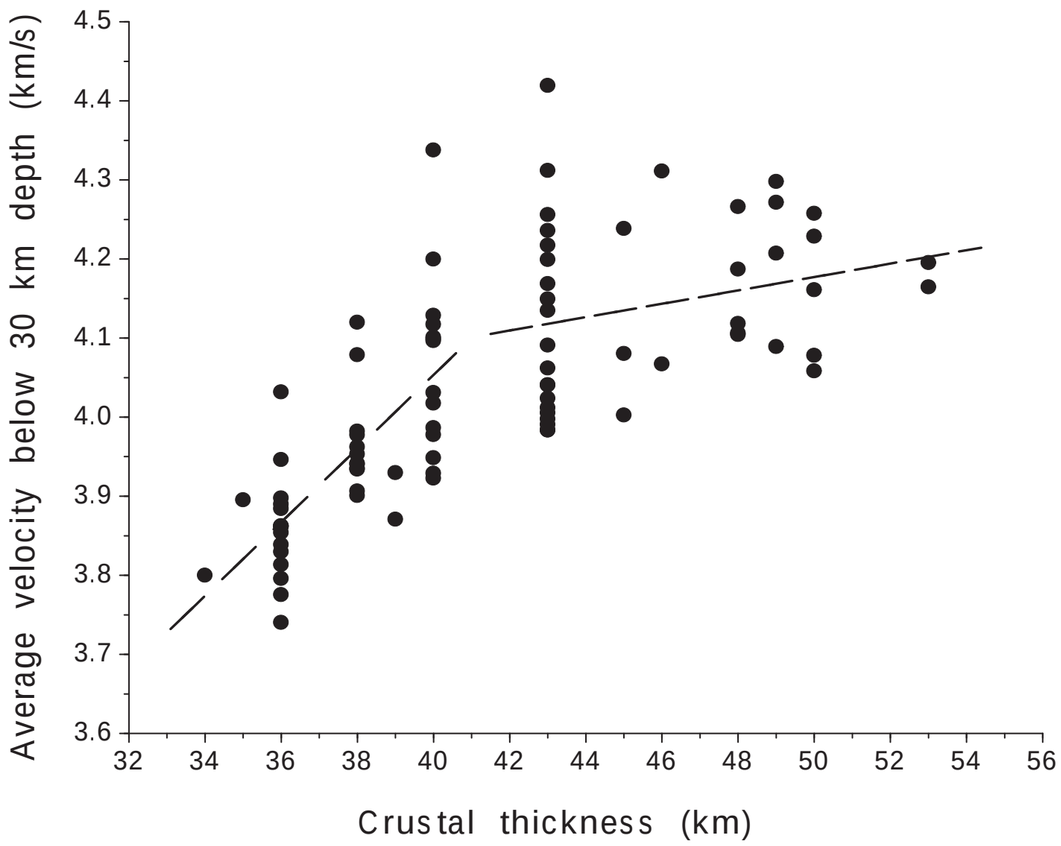
Average velocity below 30 km depth (km/s)
4.5
4.4
4.3
4.2
4.1
4.0
3.9
3.8
3.7
3.6
32
34
36
38
40
42
44
46
48
50
52
54
56
Crustal thickness (km)

Figure 11

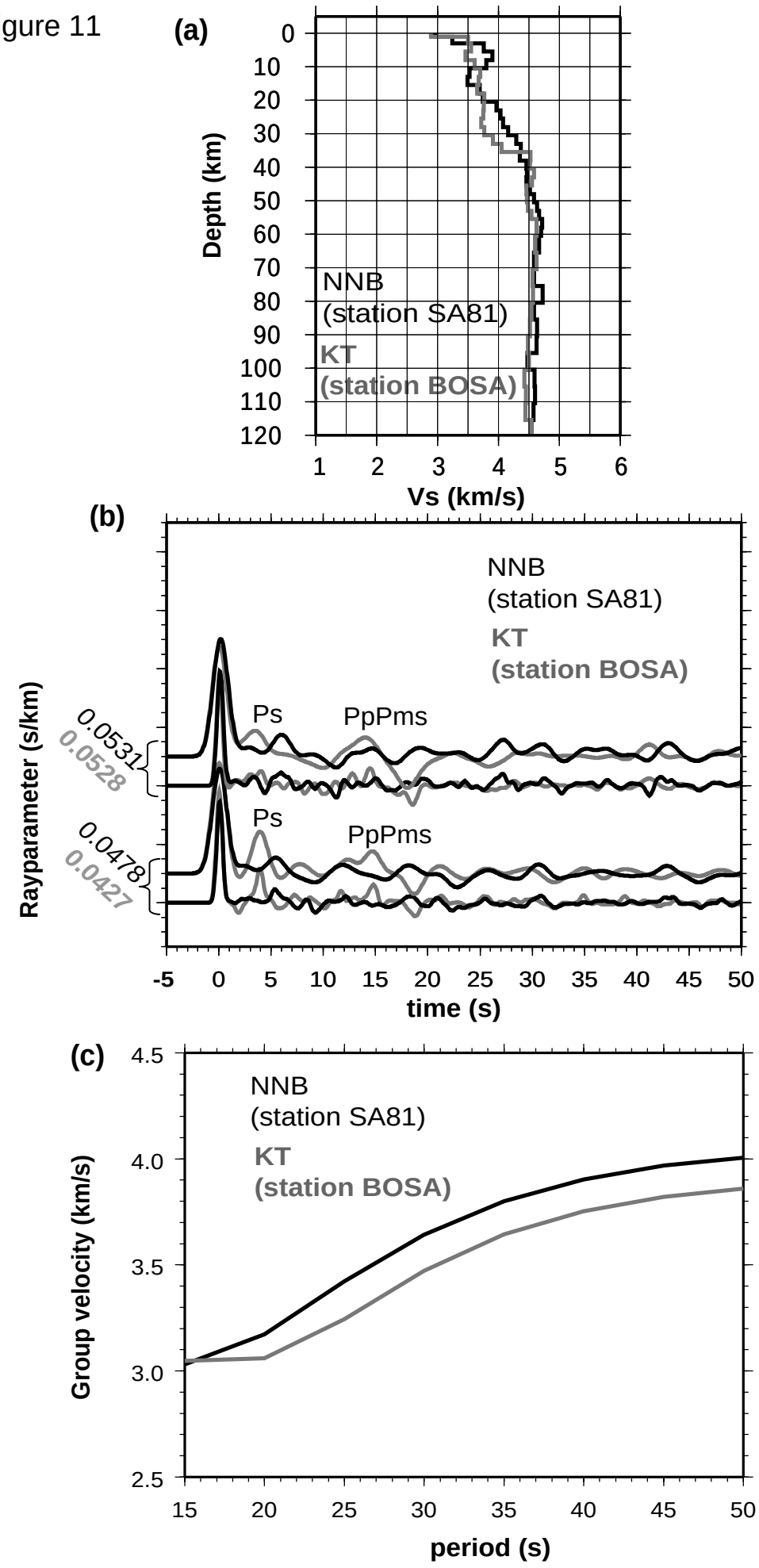
(a)
Depth (km)
0
10
20
30
40
50
60
70
80
90
100
110
120
NNB
(station SA81)
KT
(station BOSA)
1
2
3
4
5
6
Vs (km/s)
(b)
Rayparameter (s/km)
NNB
(station SA81)
KT
(station BOSA)
Ps
PpPms
0.0531
0.0528
Ps
PpPms
0.0478
0.0427
-5
0
5
10
15
20
25
30
35
40
45
50
time (s)
(c)
Group velocity (km/s)
4.5
4.0
3.5
3.0
2.5
NNB
(station SA81)
KT
(station BOSA)
15
20
25
30
35
40
45
50
period (s)

Figure 12

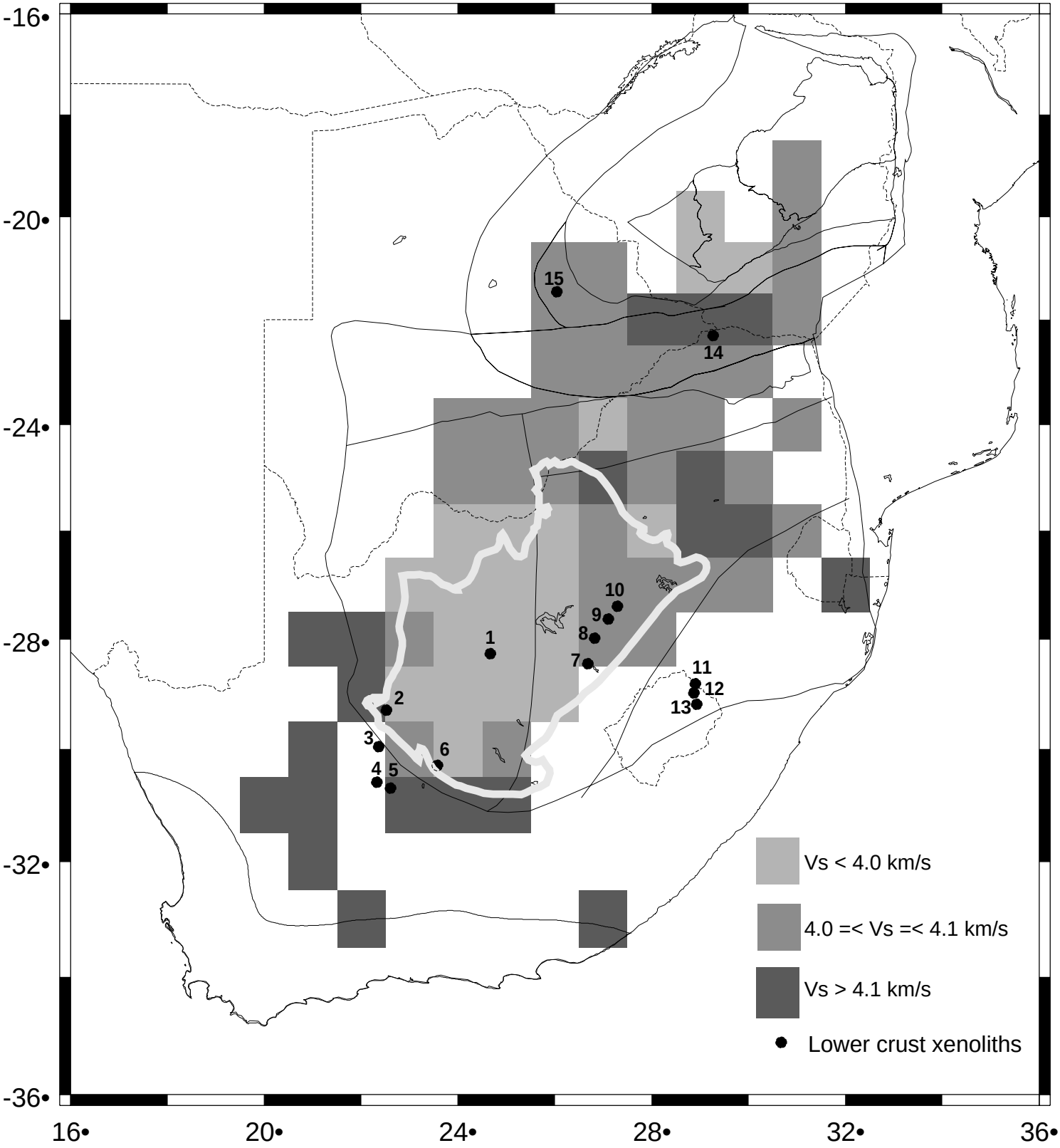
-16•
-20•
-24•
-28•
-32•
-36•
16•
20•
24•
28•
32•
36•
15
14
10
9
8
7
1
11
12
13
2
3
6
4
5
Vs < 4.0 km/s
4.0 =< Vs =< 4.1 km/s
Vs > 4.1 km/s
Lower crust xenoliths